Primate-specific BTN3A2 protects against SARS-CoV-2 infection by interacting with and reducing ACE2

Ling Xu[1,2,3,*], Dandan Yu[1,2,3], Min Xu[1,2], Yamin Liu[1,2], Lu-Xiu Yang[1], Qing-Cui Zou[3], Xiao-Li Feng[3], Ming-Hua Li[3], Nengyin Sheng[1,2,*], Yong-Gang Yao[1,2,3,4,*]

[1] Key Laboratory of Genetic Evolution and Animal Models, Key Laboratory of Animal Models and Human Disease Mechanisms of Yunnan Province, and KIZ/CUHK Joint Laboratory of Bioresources and Molecular Research in Common Diseases, Kunming Institute of Zoology, Chinese Academy of Sciences, Kunming, 650204, China

[2] Kunming College of Life Science, University of Chinese Academy of Sciences, Kunming, 650204, China

[3] Kunming National High-Level Biosafety Research Center for Non-Human Primates, Center for Biosafety Mega-Science, Kunming Institute of Zoology, Chinese Academy of Sciences, Kunming, 650107, China

[4] National Research Facility for Phenotypic & Genetic Analysis of Model Animals (Primate Facility), National Resource Center for Non-Human Primates, Kunming Institute of Zoology, Chinese Academy of Sciences, Kunming, 650107, China

[*] Corresponding authors: Dr. Yong-Gang Yao, E-mail: yaoyg@mail.kiz.ac.cn or Dr. Ling Xu, E-mail: xuling0502@mail.kiz.ac.cn or Dr. Nengyin Sheng, E-mail: shengnengyin@mail.kiz.ac.cn

Summary

Background Coronavirus disease 2019 (COVID-19) is an immune-related disorder caused by severe acute respiratory syndrome coronavirus 2 (SARS-CoV-2). The complete pathogenesis of the virus remains to be determined. Unraveling the molecular mechanisms governing SARS-CoV-2 interactions with host cells is crucial for the formulation of effective prophylactic measures and the advancement of COVID-19 therapeutics.

Methods We analyzed human lung single-cell RNA sequencing dataset to discern the association of butyrophilin subfamily 3 member A2 (*BTN3A2*) expression with COVID-19. The *BTN3A2* gene edited cell lines and transgenic mice were infected by live SARS-CoV-2 in a biosafety level 3 (BSL-3) laboratory. Immunoprecipitation, flow cytometry, biolayer interferometry and competition ELISA assays were performed in *BTN3A2* gene edited cells. We performed quantitative real-time PCR, histological and/or immunohistochemical analyses for tissue samples from mice with or without SARS-CoV-2 infection.

Findings The *BTN3A2* mRNA level was correlated with COVID-19 severity. *BTN3A2* expression was predominantly identified in epithelial cells, elevated in pathological epithelial cells from COVID-19 patients and co-occurred with *ACE2* expression in the same lung cell subtypes. BTN3A2 targeted the early stage of the viral life cycle by inhibiting SARS-CoV-2 attachment through interactions with the receptor-binding domain (RBD) of the Spike protein and ACE2. BTN3A2 inhibited ACE2-mediated SARS-CoV-2 infection by reducing ACE2 *in vitro* and *in vivo*.

Interpretation These results reveal a key role of BTN3A2 in the fight against COVID-19. Identifying potential monoclonal antibodies which mimic BTN3A2 may facilitate disruption of SARS-CoV-2 infection, providing a therapeutic avenue for COVID-19.

Funding This study was supported by the National Natural Science Foundation of China (32070569, U1902215, and 32371017), the CAS "Light of West China" Program, and Yunnan Province (202305AH340006).

Keywords: BTN3A2, SARS-CoV-2, Spike protein, ACE2, COVID-19

Research in context

Evidence before this study

Our understanding of the pathogenesis of COVID-19, especially key molecular events in the early stage of viral infection, remains incompletely albeit we witnessed many progresses. This knowledge gap hinders the finding for effective and specific antiviral agents against SARS-CoV-2. The entry of SARS-CoV-2 is mediated by the entry receptor angiotensin-converting enzyme 2 (ACE2) and is affected by host antiviral defenses. Targeting these universal host factors required for virus replication is the most promising approach for effective prevention and treatment of COVID-19.

Added value of this study

Our study revealed that *BTN3A2,* a primate-specific gene, acts as a potent inhibitor of SARS-CoV-2 infection *in vitro* and *in vivo*. The up-regulation of BTN3A2 upon SARS-CoV-2 infection competed with the ACE2 receptor for binding to the Spike protein, subsequently reducing ACE2 expression and ACE2-mediated SARS-CoV-2 entry.

Implications of all the available evidence

These data highlighted that BTN3A2 as a novel host factor with protective effects against SARS-CoV-2 infection. The BTN3A2 holds considerable potential as a therapeutic drug for mitigating the impact of SARS-CoV-2 and its variants of concern (VOCs).

Introduction

The emergence of coronavirus disease 2019 (COVID-19), caused by severe acute respiratory syndrome coronavirus 2 (SARS-CoV-2), precipitated a global pandemic with persistent pathological sequelae [1, 2]. According to the World Health Organization, the pandemic resulted in more than 6.9 million deaths in recent years [3], posing a significant threat to global health and economic security [4]. SARS-CoV-2 induces extensive damage to multiple organ systems via an overactive host immune response [5, 6]. To date, a lot of research efforts have focused on the development of pan-sarbecovirus vaccines and neutralizing antibodies [7]. However, the pathogenesis of COVID-19, especially key molecular events in the early stage of viral infection, remains incompletely understood. This knowledge gap contributes to the limited availability of effective and specific antiviral agents against SARS-CoV-2 [8-10]. Therefore, further efforts are required to clarify host-virus interactions and viral pathogenesis and thus identify candidate targets for the prevention and treatment of SARS-CoV-2 infection.

Receptor binding constitutes a critical step in viral invasion [11, 12]. In the case of SARS-CoV-2, the Spike protein, specifically the receptor-binding domain (RBD) in S1 subunit, mediates recognition of the host ACE2 receptor to facilitate viral entry [12-17]. Mutations in the Spike protein, particularly in the RBD, can lead to immune evasion, reduce efficacy of existing vaccines, and escape from neutralizing antibodies, as exemplified by the global spread of the Omicron variants [18-20]. Consequently, identifying broad-spectrum antiviral targets and additional candidates that are

effective against different viral variants has become a critical objective in combating the COVID-19 pandemic. Viral host receptors such as ACE2, which is indispensable for SARS-CoV-2 cellular entry, present attractive candidates for intervention [14, 21, 22]. ACE2 is a transmembrane carboxypeptidase with broad substrate specificity, including angiotensin II, which is essential for viral entry [15]. Importantly, as ACE2 is a host factor, its expression is less likely to be affected by viral mutations. This suggests that therapeutic approaches aimed at modulating ACE2 expression may be effective against multiple SARS-CoV-2 variants [23]. Hence, the exploration of drugs or targets that either directly or indirectly affect ACE2 to modulate SARS-CoV-2 infection represents a viable strategy for investigation.

The butyrophilin subfamily 3 (*BTN3*) is a member of the immunoglobulin transmembrane superfamily [24, 25], which is gaining increased attention. The three primary members of the BTN3A family, BTN3A1, BTN3A2, and BTN3A3, share similar extracellular domains. BTN3A1 and BTN3A3 contain an intracellular B30.2 domain that is absent in BTN3A2. The *BTN3A2* is a primate-specific gene that likely evolved during primate lineage development [26]. Members of the BTN3 family members are expressed in most human immune cell subsets and are known to participate in immunomodulatory functions [27]. Recent studies reiterated that BTN3A1 plays a key role in T cell function [28-30]. BTN3A2, in particular, has been implicated in the evolutionary and development of the primate brain [31] and is associated with various psychological disorders [26, 32-34]. While fewer literatures demonstrated an association of this family member with antiviral properties, recent studies have

identified BTN3A3 as a restriction factor against Ebola virus replicons [35] and as a key barrier to avian influenza A virus spillover into humans [36], suggesting a potential involvement of the BTN3A family in modulating host antiviral defense. We got to know the *BTN3A2* gene during our initial integrative analyses for the genome-wide association data of schizophrenia [26] and major depressive disorder [34], and this gene was featured as a risk gene for these mental disorders. We accidently found that overexpression of BTN3A2 could inhibit SARS-CoV-2 replication in Calu-3 cells when we studied SARS-CoV-2 [37-42]. Reanalysis of reported data in a subsequent study by Li et al. [43] showed up-regulation of the mRNA levels of *BTN3A2* and *BTN3A3*, along with other related genes in Calu-3 cells upon SARS-CoV-2 infection. All these observations suggested that BTN3A2 may play a potent role in host antiviral defense against SARS-CoV-2, though the precise mechanism underlying this regulation remains to be clarified.

In this study, we assessed the potential role of BTN3A2 as a key host factor in combating SARS-CoV-2 infection. Based on publicly available datasets and newly obtained data, we observed an up-regulation of *BTN3A2* mRNA expression in COVID-19 patients and non-human primates (NHPs). Using cellular and animal models of SARS-CoV-2 infection, we also established that BTN3A2 competed with the ACE2 via directly interacting with the SARS-CoV-2 Spike RBD, thereby reducing ACE2 receptor expression and ACE2-mediated SARS-CoV-2 entry. This study identified BTN3A2 as a host factor against SARS-CoV-2 infection, providing a basis for the development of potential small molecule inhibitors targeting BTN3A2 for the

treatment of COVID-19.

Materials and Methods

Ethics statement

The ethics review board of the Kunming Institute of Zoology (KIZ), Chinese Academy of Sciences (CAS) approved this study. All animal experiments were approved by the Ethics Committee of KIZ, CAS (approval number IACUC-RE-2023-03-004). All experiments involving live SARS-CoV-2 were conducted in the animal biosafety level 3 (ABSL-3) facility at KIZ, CAS (approval numbers KIZP3-XMZR-2021-23 and KIZP3-XMZR-2023-04).

Viral strains and cells

The SARS-CoV-2 prototype was kindly provided by the Guangdong Provincial Center for Disease Control and Prevention (Guangdong, China), as described in our previous studies [37-39]. The virus was amplified in Vero-E6 cells and median tissue culture infective dose ($TCID_{50}$) was used to assess viral infectivity. The viral sequence is accessible from the China National Microbiology Data Center (NMDC, Accession No. NMDCN0000HUI). The SARS-CoV-2 variant BA.2 was isolated from a patient in Yunnan Provincial Infectious Disease Hospital and its sequence is accessible at NMDC (Accession No. NMDC60046377) [44]. Virions from the fourth passage were used in all experiments. The VSV-G pseudotyped viruses (G*ΔG-VSV-Rluc),

containing prototype and variant BA.1 [44], were kindly provided by Prof. Yong-Tang Zheng at KIZ, CAS. The VSV-G pseudotyped viruses (VSV*ΔG-GFP), co-expressing SARS-CoV-2 spike protein and a green fluorescent protein (GFP) reporter [42], were kindly provided by Prof. Qihui Wang at Institute of Microbiology, CAS. All viruses were preserved at -80°C freezer.

The HEK293T, Huh7, A549, and Vero E6 cells were obtained from the Kunming Cell Bank, KIZ, and were grown in Dulbecco's Modified Eagle Medium (DMEM, high glucose;11965-092, Gibco-BRL, USA) supplemented with 10% fetal bovine serum (FBS, Gibco-BRL,10099-141) and 1% penicillin/streptomycin (15140122, Gibco-BRL, USA). The Calu-3 cells were purchased from Procell Life Science & Technology Co., Ltd, and were cultured in Minimum Essential Medium (MEM; 11095080, Gibco-BRL, USA) supplemented with 10% FBS (Gibco-BRL,USA), 1% MEM non-essential acids (11140050, Gibco-BRL, USA), 1% sodium pyruvate (100 mM, 11360070, Gibco-BRL, USA), and 1% antibiotics. All cells were cultured at 37 °C in a humidified atmosphere of 5% CO_2, and were used for different purposes of testing.

Plasmid construction and transfection

Two transcripts of human *BTN3A2* (encoding BTN3A2 long isoform [BTN3A2-L] and short isoform [BTN3A2-S]) were cloned into Flag-tagged pCMV-3Tag-8, as described in our previous report [26]. Briefly, the coding region of *BTN3A2* was sub-cloned into a pCMV-3Tag-8-His vector using the same primers and sub-cloned into

186 pCMV-HA (Clontech, PT3283-5) using *Eco*R I/*Xho* I (New England Biolabs, USA).
187 The expression vector for the SARS-CoV-2 Spike protein (pCMV3-2019-nCoV-Spike
188 (S1+S2)-long) was purchased from Sino Biological (VG40589-UT, China). The
189 expression vector for ACE2 was purchased from Miaolinbio (pEnCMV-ACE2
190 (human)-3×FLAG, P16698, China). The expression vectors for the Spike S1 (S-S1)
191 and Spike S2 subunits (S-S2) were reported in our previous study [45]. The expression
192 vector for the prototype RBD (pEnCMV-RBD (SARS-CoV-2)-3×FLAG) was
193 purchased from Miaolinbio (P15640, China), while the expression vectors for the
194 SARS-CoV-2 variant RBDs of the S1 subunit (including α, γ, δ, BA.1, BA.2,
195 BA.2.12, and BA.5) were kindly provided by Prof. Jinghua Yan at Institute of
196 Microbiology, CAS. All primers used to construct plasmids were listed in
197 Supplementary Table S1. Each construct was verified by direct Sanger sequencing.
198 The HEK293T (ACE2-293T) and A549 (ACE2-A549) cells with stable
199 expression of ACE2 were transfected using Lipofectamine™ 3000 (L3000008,
200 Invitrogen, USA) following the manufacturer's protocols to test the antiviral activity
201 during SARS-CoV-2 infection. In brief, the cells were cultured in 12-well plates and
202 grown to 70% confluence. The cells in each well were then transfected with 125 μL of
203 solution containing 1 μg of plasmid DNA, 125 μL of Opti-MEM medium (31985-070,
204 Gibco-BRL,USA), and 5 μL of Lipofectamine™ 3000. Cells were incubated with the
205 transfection mixture for 6 h at 37 °C in a humidified atmosphere of 5% CO_2, then the
206 medium changed to growth medium.
207

208 **Generation of genetically modified cell lines**

209 We used Huh7 and Calu-3 cells, which have a moderate expression of *BTN3A2*
210 mRNA and can be naturally infected by SARS-CoV-2, to establish cell lines with
211 BTN3A2 knockout. In brief, two single-guide RNAs (sgRNAs) (sgBTN3A2 #1:
212 TGTTCTCTCCCTTGGCGTTGCTCCACTGTA; sgBTN3A2 #3:
213 ATCATGAGAGGCGGCTCCGGGGAGGGTGTATC) targeting different coding
214 regions of the *BTN3A2* gene were cloned into linearized lentiCRISPRv2 (#52961,
215 Addgene, USA). Lipofectamine™ 3000 transfection reagent in Opti-MEM medium
216 was used to co-transfect HEK293T cells with psPAX2 (#12260, Addgene, USA),
217 pMD2.G (# 12259, Addgene, USA), and indicated individual sgRNA constructs at a
218 ratio of 2:1:3, in accordance with the manufacturer's instructions. Transfection
219 medium was replaced with viral production medium at 6 h after transfection. The
220 supernatants of the respectively transfected HEK293T cells were collected at 72 h
221 after transfection and filtered using a 0.45 μm filter (SLHV033RB, Millipore, USA).
222 Huh7 and Calu-3 cells were transduced with 1 mL of the above harvested lentiviral
223 stock with polybrene (1 mg/mL, H8761, Solarbio, China) for 24 h. The cells were
224 then switched to 2 mL of fresh medium and puromycin (1 μg/mL, A1113803, Gibco-
225 BRL, USA) to select for successfully transduced Huh7 and Calu-3 cells. We obtained
226 two strains of Huh7 cell with BTN3A2 knockout (sgBTN3A2-1 Huh7 cell and
227 sgBTN3A2-3 Huh7 cells) and two strains of Calu-3 cell with BTN3A2 knockout
228 (sgBTN3A2-1 Calu-3 cell and sgBTN3A2-3 Calu-3 cell), respectively, after
229 verification by using Western blot for the knockout of BTN3A2. The lentiviral

230 particle (sgNC; generated by transfecting HEK293T cells with the lentiCRISPRv2
231 empty vector, psPAX2, and pMD2.G) was used to establish control cell lines (sgNC
232 Huh7 cells and sgNC Calu-3 cells) for those Huh7 cell and Calu-3 cells with BTN3A2
233 knockout.

234 We also established Huh7 cell and Calu-3 cells with stable expression of the
235 BTN3A2 isoforms (BTN3A2-L and BTN3A2-S) [26] using the TETon system (632162,
236 Clontech, USA), respectively. Briefly, the coding region sequence of the BTN3A2-L
237 or BTN3A2-S was sub-cloned from pCMV-HA-BTN3A2-L and pCMV-HA-
238 BTN3A2-S expression vectors into the pLVX-tight-puro vector (632162, Clontech,
239 USA) (Supplementary Table S1). The TETon system was combined with a separate
240 lentiviral compatible vector containing the reverse tetracycline-controlled
241 transactivator Advance (rtTA Advance) (632163, Clontech, USA). Lentiviral particles
242 corresponding to either TETon system or rtTA Advance were generated using the
243 above procedures. Huh7 and Calu-3 cells were co-transduced with the TETon system
244 containing the indicated targets (pLVX-Vector to make control cells, pLVX-BTN3A2-
245 L and pLVX-BTN3A2-S for overexpression of BTN3A2-L and BTN3A2-S,
246 respectively) and rtTA Advance lentiviral particles (each 1 mL) in the presence of
247 polybrene (1 mg/mL) for 48 h. The culture medium was replaced with 2 mL of fresh
248 medium and incubated for an additional 24 h. Cells were subsequently selected using
249 G418 (250 ng/mL, A1720, Sigma-Aldrich) and puromycin (1 μg/mL) for a minimum
250 of two weeks. We obtained a total of four strains with stable expression of BTN3A2
251 isoform (Huh7 cells: BTN3A2-L Huh7 and BTN3A2-S Huh7; Calu-3 cells: BTN3A2-

L Calu-3 and BTN3A2-S Calu-3) and two strains of control cells (Vector Huh7 and Vector Calu-3).

To generate cell lines with a stable ACE2 expression, we used HEK293T cells and A549 cells, as both have a high transfection efficiency and a high SARS-CoV-2 infection efficiency after stable overexpression of ACE2. Briefly, a lentiviral expression system for ACE2 was established using the pLenti-CMV-ACE2-Flag plasmid (Public Protein/Plasmid Library, China) in HEK293T cells, and viral particles in the supernatants were collected. For lentiviral expression of ACE2, both HEK293T and A549 cells were seeded in 6-well plates and transduced by infection mixture containing 1 mL of culture medium with 1 μg of polybrene (H8761, Solarbio, China) and 1 mL of viral supernatants. Subsequently, the culture medium was replaced with 2 mL of fresh medium containing puromycin (1 μg/mL) to select for successfully transduced HEK293T and A549 cells overexpressing ACE2. The cell lines with stable expression of ACE2 (ACE2-A549 cells and ACE2-HEK293T cells) were verified by Western blot.

Western blotting and immunoprecipitation

Western blotting and immunoprecipitation were performed using the same procedures described in our previous studies [46, 47]. In brief, cells were lysed on ice in RIPA lysis buffer (P0013, Beyotime Institute of Biotechnology, China) and centrifuged at 12 000 *g* for 5 min at 4 °C to harvest cell lysates. Protein concentration was determined using a BCA Protein Assay Kit (P0012, Beyotime Institute of Biotechnology, China).

Bovine serum albumin (BSA; P0007, Beyotime Institute of Biotechnology, China) was used as the protein standard. Cell lysates (20 μg of total protein/sample) were separated by 12% sodium dodecyl-sulfate polyacrylamide gel electrophoresis (SDS-PAGE), before transfer to polyvinylidene fluoride (PVDF) membranes (IPVH00010, Roche Diagnostics, China) using standard procedures. The membranes were then blocked with 5% non-fat dry milk in Tris-buffered saline (#9997, Cell Signaling Technology, USA) with 0.1% Tween 20 (P1379, Sigma, USA) (TBST) at room temperature for 2 h. Membranes were incubated with primary antibodies against His (1:5 000, M20001M, Abmart, China), HA (1:5 000, M20003M, Abmart, China), Flag (1:5 000, M20008M, Abmart, China), ACE2 (1:1 000, 66699-1-Ig, Proteintech, China), BTN3A2 (1:1 000, TA500730, Origene, USA), Spike (1:1 000, 28869-1-AP, Proteintech, China), and Tubulin (1:10 000, OTI3H2, ZSGB-Bio, China) overnight at 4 °C, respectively. The membranes were washed three times (5 min each) with TBST and incubated with TBST-conjugated anti-mouse (5450-0011) or anti-rabbit (5220-0458) secondary antibody (1:10 000, Milford, MA, USA) for 1 h at room temperature. After washing with TBST three times, the proteins on the membranes were detected by enhanced chemiluminescence reagents (WBKLS0500, Millipore, USA). All antibodies have been validated in our previous studies [37, 38, 46, 48] or using the western blot assays in this study.

For immunoprecipitation, appropriate antibodies were incubated with protein G-agarose beads (15920010, Life Technologies, USA) to form a complex for 2 h at room temperature. Cells were lysed with RIPA lysis buffer on ice for 1 h, followed by

centrifugation at 12 000 *g* for 10 min at 4 °C. The lysates were then immunoprecipitated with the complex at 4 °C overnight, followed by four washes with RIPA lysis buffer and resuspension in loading sample buffer for SDS-PAGE.

Syncytia formation assay

The syncytia formation assay was performed by using a co-culture system of Huh7 cells and HEK293T cells, following a previously described procedure [49, 50]. Briefly, Huh7 cells with overexpression of BTN3A2-L or BTN3A2-S, and control cells (Vector Huh7 cells) were seeded in a 4-well chamber slide (Nunc™ Lab-Tek™ II, 177399, Thermo Scientific, USA) at a density of 1×10^4 cells/ well for overnight culture, then were transfected with the pX-330 plasmid (Addgene) (500 ng/well) using Lipofectamine™ 3000 (L3000008, Invitrogen, USA) for 16 h to be ready for the syncytia formation assay. The HEK293T cells were cultured in a 12-well plate to approach 60-70% confluence and were transfected with expression vector for Spike of SARS-CoV-2 Delta [44] (1 μg) for 16 h, then cells were trypsinized and re-suspended in DMEM supplemented with 5% FBS at a density of 2×10^4 cells/mL. We seeded HEK293 cell suspension (500 μL/well) into the 4-well chamber slide with the above prepared Huh7 cells (BTN3A2-L, BTN3A2-S, and Vector Huh7 cells) for co-culture for 20 h. Cells were collected and fixed with 4% paraformaldehyde (PFA, 158127, Sigma-Aldrich, USA) for further immunofluorescence assay.

Immunofluorescence

318 Huh7 cells with BTN3A2 overexpression (BTN3A2-L and BTN3A2-S Huh7 cells) or
319 knockout (sgBTN3A2-1 and sgBTN3A2-3 Huh7 cells) and corresponding control
320 cells (Vector Huh7 and sgNC Huh7) were seeded on glass coverslips and grown
321 overnight to 40% confluence in DMEM supplemented with 10% FBS at 37 ^{o}C in 5%
322 CO_2. The BTN3A2-L and BTN3A2-S Huh7 cells were treated with Dox (1 mg/mL,
323 D9891, Sigma-Aldrich, USA) for 24 h to induce the expression of BTN3A2 isoform.
324 All cultured cells were infected with the VSV*ΔG-GFP SARS-CoV-2 S for 24 h
325 before harvest for immunofluorescence analysis. Cells were fixed with 4%
326 paraformaldehyde for 10 min and were incubated with mouse anti-BTN3A2 (1:50)
327 overnight at 4 ^{o}C. After three washes with phosphate-buffered saline (PBS) with 0.1%
328 Tween 20 (PBST; 5 min each), immunoreactivity was detected by using the FITC-
329 conjugated secondary antibody (1:500; KPL, 172-1506; incubation for 1 h at room
330 temperature). Nuclei were counterstained with 1 μg/mL DAPI (Roche Diagnostics,
331 10236276001) and the slides were visualized under an Olympus FluoView™ 1000
332 confocal microscope.
333
334 **Flow cytometry**
335 To measure the cell surface expression level of ACE2, Huh7 cells and Calu-3 cells
336 with BTN3A2 overexpression (BTN3A2-L Huh7 cells, BTN3A2-S Huh7 cells,
337 BTN3A2-L Calu-3 cells and BTN3A2-S Calu-3 cells) or knockout (sgBTN3A2-1
338 Huh7 cells, sgBTN3A2-3 Huh7 cells, sgBTN3A2-1 Calu-3 cells, and sgBTN3A2-3
339 Calu-3 cells), and corresponding control cells (Vector Huh7, Vector Calu-3, sgNC

340 Huh7, and sgNC Calu-3) were washed with PBS and stained with mouse anti-ACE2
341 (66699-1-Ig, Proteintech, China) at a 1:50 dilution for 30 min at 4 °C. The cells were
342 then washed twice and re-suspended in 1×PBS containing secondary antibody
343 (AF647-labeled donkey anti-goat immunoglobulin G (IgG), A31571, Invitrogen,
344 USA) at a 1:500 dilution. After 30 min of incubation at 4 °C, the cells were washed
345 twice and re-suspended in 1×PBS before flow cytometry analysis using FACSCelesta
346 (BD Biosciences, USA). Data were analyzed using FlowJo software.
347

348 **Re-analysis of RNA-sequencing (RNA-seq) datasets**

349 RNA-seq data of blood leukocytes collected from 26 hospitalized non-COVID-19
350 patients and 100 COVID-19 patients with different degrees of disease severity were
351 obtained from the Gene Expression OmniBus (GEO, www.ncbi.nlm.nih.gov/geo/,
352 accession number GSE157103) [51]. Of these individuals, 16 non-COVID-19 patients
353 and 50 COVID-19 patients were admitted to the intensive care unit (ICU). The RNA-
354 seq dataset of monocytic-myeloid-derived suppressor cells (M-MDSCs) from 12
355 COVID-19 patients (four severe, four asymptomatic, and four convalescent) and four
356 controls were downloaded from the GEO database (accession number GSE178824) [52].
357 Raw RNA-seq data of 15 tissues from three rhesus macaques (*Macaca mulatta*)
358 infected with SARS-CoV-2 and one control were downloaded from the China
359 National Center for Bioinformation (https://www.cncb.ac.cn/) (accession number
360 CRA004025) [53]. The raw sequencing reads were first cleaned using Trimmomatic
361 v0.33 [54], then mapped to the rhesus macaque reference genome (Mmul_10,

362 https://www.ncbi.nlm.nih.gov/datasets/genome/GCF_003339765.1/) using STAR
363 v2.7.3a [55]. Gene expression quantification was conducted with RSEM v1.3.1 [56].
364 Single-cell RNA-seq (scRNA-seq) data of peripheral blood from five healthy
365 donors and 27 COVID-19 patients were downloaded from
366 https://atlas.fredhutch.org/fredhutch/covid/dataset/merged [57]. ScRNA-seq data of lung
367 tissues from seven controls and 19 COVID-19 patients were downloaded from
368 https://singlecell.broadinstitute.org/single_cell/study/SCP1219/columbia-university-
369 nyp-covid-19-lung-atlas [58]. The expression levels of *BTN3A2* and *ACE2* in bulk non-
370 disease human tissues and single cells were obtained from the GTEx Portal
371 (https://www.gtexportal.org/) [59, 60]. RNA-seq data of mock (n=3) and SARS-CoV-2
372 (n=3)-infected lung-derived Calu-3 cells, primary human lung epithelial cells (NHBE)
373 and lung biopsies from healthy controls (n=2) and postmortem COVID-19 patients
374 (n=2) were obtained from the GEO database (accession number GSE147507) [61, 62].
375 Raw counts were normalized using DESeq2 [63] and batch effects among samples were
376 removed using the removeBatchEffect function from limma [64]. For bulk RNA-seq
377 data, the *BTN3A2* expression levels were compared between different groups using
378 two-sided t-tests. For scRNA-seq data, the *BTN3A2* expression levels were compared
379 between different groups for each cell type using two-sided Wilcox rank sum tests.
380 Expressional correlations between two genes were calculated using Pearson's
381 correlation.
382
383 **Animals and tissues**

Left lobe lung tissue from rhesus macaques (*n*=6) [65] and cynomolgus macaques (*Macaca fascicularis*; *n*=8) [66] infected with SARS-CoV-2 were obtained from the tissue bank of the ABSL-3 facility at KIZ, CAS. Lung tissues from healthy rhesus macaques (*n*=5) and cynomolgus macaques (*n*=6) were purchased from the National Resource Center for Non-Human Primates, KIZ.

C57BL/6J wild-type (WT) mice were obtained from the experimental animal core facility of KIZ, CAS. Humanized *BTN3A2* knock-in mice were generated using CRISPR/Cas9 on a C57BL6/J background by inserting the coding sequence of the human *BTN3A2* gene (Transcript ID: ENST00000356386.6) with a HA-tag in its N-terminus into the *Hipp11* (*H11*) locus. The BTN3A2 transgenic (BTN3A2-tg) mice were created by GemPharmatech (Nanjing, China). Both male and female mice (4 weeks) were used for the experiments. All mice were genotyped by PCR with genomic DNA prepared from tail tips using primer pair 5'-CAGCAAAACCTGGCTGTGGATC-3' / 5'-CGTAGATGTACTGCCAAGTAGG-3'. Mice were housed in clear plastic cages and bred in a specific pathogen-free condition at the experimental animal core facility of KIZ, with free access to water and food under 22 ± 2 ºC, 50 % humidity, and 12 h light/dark cycle.

Animal models for SARS-CoV-2 infection

To evaluate whether adeno-associated virus (AAV) exhibits good efficiency for overexpressing exogenous protein in mouse tissues, we infected four age-matched C57BL/6J (*n*=2) and BTN3A2-tg (*n*=2) mice with enhanced green fluorescent protein

406 (EGFP)-expressing AAV (AAV-EGFP) (PackG410ene Biotech, Guangzhou, China).
407 Briefly, mice were intranasally infected with AAV-EGFP (PackGene Biotech,
408 Guangzhou, China) at a total volume of 30 μL containing 2×10^{12} viral genome copies.
409 The AAV-EGFP-infected mice were sacrificed at 14 days post-infection (dpi) with
410 AAV.

411 A total of 6-10 mice per group were used for infection according to our previous
412 study [41]. Human ACE2 (hACE2) was overexpressed using hACE2-expressing AAV
413 (AAV-hACE2) in C57BL/6J (*n*=9) mice and BTN3A2-tg mice (*n*=8). In brief, mice
414 were intranasally infected with AAV-hACE2 (PackGene Biotech, Guangzhou, China)
415 at a total volume of 30 μL containing 2×10^{12} genome copies. The C57BL/6J (*n*=7)
416 and BTN3A2-tg (*n*=6) mice were monitored daily until SARS-CoV-2 infection at 14
417 dpi with AAV-hACE2. After anesthetization with isoflurane (RWD Life Science,
418 China), the mice were intranasally infected with a total volume of 30 μL containing
419 1×10^{5} $TCID_{50}$ of SARS-CoV-2 variant BA.2. All infected animals were housed at the
420 ABSL-3 facility on a 12 h light/dark cycle, with free access to food and water, and
421 were sacrificed at 3 dpi. The remaining C57BL/6J (*n*=2) and BTN3A2-tg (*n*=2) mice
422 with AAV-hACE2 infection but without SARS-CoV-2 infection were assigned as the
423 control group and sacrificed at 14 dpi with AAV.

424 Tissue samples were collected from all animals after euthanasia and stored in a
425 −80 °C freezer (for quantification of mRNA and protein levels) or in 4% PFA (for
426 histological analysis and immunochemistry) until use.

427

428 **Measurement of viral RNAs**

429 RNA copies per mL (cell RNA) or per μg (lung samples) were determined by
430 quantitative real-time polymerase chain reaction (qRT-PCR), as described in our
431 previous study [38]. Briefly, total RNA was extracted from 200 μL of indicated cell
432 supernatants using a High Pure Viral RNA Kit (11858882001, Roche, Germany). The
433 extracted RNA was eluted in 50 μL of elution buffer. TRIzol Reagent (15596026CN,
434 Thermo Fisher Scientific, USA) was used for total RNA isolation from cells and
435 homogenized tissues. Viral RNA copies were detected using a THUNDERBIRD
436 Probe One-Step qRT-PCR Kit (QRZ-101, TOYOBO, Japan). A total of 25 μL reaction
437 solution, containing 8.7 μL of extracted RNA from indicated cell supernatant or 1 μg
438 of total RNA from cells or lung tissue samples, was prepared for qRT-PCR analysis [38].
439 The Applied Biosystems 7500 Real-Time PCR system was used for qRT-PCR
440 analysis with the following thermal cycle conditions: 10 min at 50 °C for reverse
441 transcription, 60 s at 95 °C, followed by 40 cycles at 95 °C for 15 s and 60 °C for 45
442 s. In each run, serial dilutions of the SARS-CoV-2 RNA reference standard (National
443 Institute of Metrology, China) were used in parallel to calculate copy numbers in each
444 sample.

445

446 **Pathological analysis**

447 The lungs of SARS-CoV-2-infected mice were fixed in 4% PFA for 7 days, processed
448 in paraffin (Leica EG1160, Germany), sectioned to 3-4 μm thickness (Leica RM2255,
449 Germany), and stained with hematoxylin and eosin (H&E), as described in our

450 previous studies [37, 38]. The slices were imaged using a Nikon Eclipse E100 microscope
451 (Japan) and were evaluated in a blinded manner by two pathologists.
452 Immunohistochemical analysis of lung tissue was performed based on previously
453 described procedures [37, 48]. In brief, each section was baked at 65 °C for 30 min,
454 followed by deparaffinization using xylene and subsequent hydration with decreasing
455 concentrations of ethanol (100% to 75%). Heat-induced antigen retrieval was
456 performed using sodium citrate buffer (pH 6.0). Endogenous peroxidase was blocked
457 with 3% hydrogen peroxide for 25 min, and non-specific binding was blocked with
458 3% BSA for 30 min at room temperature. Specimens were incubated overnight at 4 °C
459 with rabbit anti-SARS-CoV-2 nucleocapsid protein (1:200, 26369, Cell Signaling
460 Technology, USA), mouse anti-ACE2 (1:1000, Proteintech,66699-1-Ig), mouse anti-
461 GFP (1:2000, sc-9996, Santa Cruz Biotechnology, USA), and mouse anti-BTN3A2
462 antibodies (1:50, CF500730, Origene, USA), respectively. The slices were incubated
463 with mouse IgG1 kappa isotype control (1:1000, 14-4714-82, Thermo Fisher
464 Scientific, USA) as a negative control for antigen staining. After washing with PBS
465 with 0.1% Tween 20 three times, the lung slices were incubated with anti-rabbit IgG
466 (GB111738, Servicebio, China) or anti-mouse IgG secondary antibody (GB111739,
467 Servicebio, China) for 50 min at room temperature and visualized with 3,3'-
468 diaminobenzidine tetrahydrochloride. The slices were counterstained with
469 hematoxylin, dehydrated and mounted on a slide, and imaged under an Olympus
470 OlyVIA microscope (Japan).
471 For immunofluorescence assay, lung tissue sections were blocked in PBST

472 supplemented with 5% BSA for 1 h, followed by an incubation with primary anti-
473 mouse ACE2 (1:1000; Proteintech,66699-1-Ig) and anti-rabbit HA-Tag (1:800; Cell
474 signaling technology, C29F4) for 16 h. After three washes with PBST (each 5 min),
475 sections were incubated with a FITC-conjugated anti-Rabbit IgG (1:500; Life
476 Technologies, A21207) or anti-mouse IgG (1:500; Invitrogen, A21202) secondary
477 antibody, and nuclei were counterstained with DAPI. The slides were visualized under
478 an Olympus FluoView™ 1000 confocal microscope (Olympus, America).
479

480 **Enzyme-linked immunosorbent assay (ELISA) competition assays**

481 Spike S1-Fc (6.25 ng/mL, 40591-V02h, Sino Biological, China) was mixed with
482 ACE2-Fc (50 ng/mL, 10108-H02H, Sino Biological, China) or Human IgG-Fc (50
483 ng/mL, 10702-HNAH, Sino Biological, China) at 4 °C overnight. The mixture was
484 then added with a series of concentrations (0, 6.25, 12.5, 25, 50 ng/mL) of BTN3A2-
485 L-His (13515-H08H, Sino Biological, China). These sample series were transferred to
486 a plate pre-coated with an antibody specific to SARS-CoV-2 S1RBD (E-EL-E605,
487 Elabscience, China). After 2 h of incubation, the plate was washed by wash buffer
488 three times. Avidin-horseradish peroxidase (HRP) conjugate was successively added
489 to each microplate well and incubated at 4 °C for 30 min. The free components were
490 then removed by washing and substrate solution was added to each well. The enzyme-
491 substrate reaction was terminated by the addition of stop solution according to the
492 manufacturer's instructions. Those wells containing different residual concentration of
493 S1-RBD, biotinylated detection antibody, and Avidin-HRP conjugate appeared blue.

494 Optical density was measured using a BioTek Synergy HT microplate reader (BioTek,
495 USA).
496
497 **Biolayer interferometry assay**
498 The biolayer interferometry assays were performed using the Octet RED96 system
499 (ForteBio, Germany). Briefly, ACE2-Fc protein (10 μg/mL) was captured on AR2G
500 Biosensors (18-5095, ForteBio, Germany) and incubated with a series of
501 concentrations of BTN3A2-L-His (62.5, 250, 1 000, and 2 000 nM). The biolayer
502 interferometry assays were performed via four steps: (i) ACE2-Fc protein loading
503 onto AR2G Biosensors (360s); (ii) baseline; (iii) association of BTN3A2-L-His to
504 determine Kon (association rate constant) (360 s); and (iv) dissociation of BTN3A2-
505 L-His to determine Kdis (dissociation constant) (360 s). The baseline and dissociation
506 steps were performed in SD buffer (pH 7.4 PBS, 0.05% Tween 20, 0.01% BSA) and
507 biosensor drifting was corrected by background subtraction. Background wavelength
508 shifts were measured in the reference biosensors only loaded with ACE2-Fc in SD
509 buffer. All steps were conducted in a shaker (1 000 rpm, 30 °C). The data were
510 analyzed and fitted in a 1:1 binding model using Octet data analysis software
511 (ForteBio v9.0). The same procedure was used to determine whether BTN3A2 binds
512 to Spike S1. Briefly, BTN3A2-L-His protein (10 μg/mL) was captured on AR2G
513 Biosensors and incubated with Spike S1-Fc (125, 250, 500, and 1 000 nM) at various
514 concentrations.
515 We also tested whether BTN3A2-S, BTN3A1 and BTN3A3 bind to Spike S1 or

516 ACE2, respectively, following the above procedure. Briefly, BTN3A2-S-His protein
517 (10 μg/mL, Zoonbio Biotechnology, China) was captured on AR2G Biosensors and
518 incubated with Spike S1-Fc (250 nM, 500 nM, and 1 000 nM) or ACE2-Fc (500 nM,
519 and 1 000 nM) at various concentrations. For biolayer interferometry assays of
520 BTN3A1-His (10 μg/mL, 15973-H08H, Sino Biological, China) and BTN3A3-His
521 (10 μg/mL, 13432-H08H, Sino Biological, China) with Spike S1-Fc (1 000 nM) or
522 with ACE2-Fc (1 000 nM), we only used one concentration because of the limited
523 amount of each protein.
524
525 **Statistical analysis**
526 All statistical analyses were performed using GraphPad Prism version 8.0.1
527 (GraphPad Software, Inc., La Jolla, CA, USA). Comparisons between different
528 groups were conducted by using one-way analysis of variance (ANOVA) with
529 Dunnett's multiple comparisons. Data are presented as mean ± SD. A P value <0.05
530 was considered as statistically significant.
531
532 **Role of the funders**
533 The funders of this study had no role in study design, sample collection, data
534 collection, data analyses, interpretation, or writing of the report.
535
536 **Results**
537

538 ***BTN3A2* was altered in COVID-19 patients and SARS-CoV-2-infected NHPs**

539 We first analyzed *BTN3A2* mRNA expression in peripheral blood mononuclear cells
540 (PBMCs) from COVID-19 patients based on published transcriptomic data [51] to
541 examine potential relevance between *BTN3A2* and SARS-CoV-2 infection. Results
542 showed a significantly increased *BTN3A2* mRNA level in COVID-19 patients (Non-
543 ICU COVID-19) compared to non-COVID-19 patients (ICU and Non-ICU)
544 (P=5.3×10^{-4}, Fig. 1a). However, in critically ill COVID-19 patients (ICU COVID-19),
545 *BTN3A2* mRNA expression was significantly reduced relative to Non-ICU COVID-19
546 patients (P=1.42×10^{-6}, Fig. 1a). In M-MDSCs from COVID-19 patients with different
547 disease severities and stages [52], no marked differences in *BTN3A2* mRNA expression
548 were found between the healthy controls and asymptomatic patients or between
549 healthy controls and convalescent patients, but expression was significantly reduced
550 in patients with severe COVID-19 relative to healthy controls (P=3.6×10^{-3}, Fig. 1b).
551 Re-analyses of scRNA-seq data of PBMCs, B cells, T cells (CD4^{+} T, CD8^{+} T, and
552 other T cells), and natural killer (NK) cells [67] also showed an up-regulation of
553 *BTN3A2* mRNA expression in most cell types in COVID-19 patients compared to
554 healthy controls (Fig. 1c).

555 The *BTN3A2* gene is expressed in various myeloid and immune cells and plays an
556 important role in the immune response[24, 27, 68]. However, the functional implications
557 of elevated *BTN3A2* expression in the lungs, which are the primary target organs for
558 SARS-CoV-2, remain to be elucidated. Hence, we first explored the expression of
559 *BTN3A2* in healthy human lung tissues using available GTEx data [59]. Results

560 indicated that the lungs had the second highest *BTN3A2* expression among 30 tested
561 tissues (Supplementary Fig. S1a). Among the different cell types in the lung tissue,
562 alveolar type 1 and 2 cells, together with alveolar macrophages, showed relatively
563 high *BTN3A2* expression (Supplementary Fig. S1b). Further analysis of the scRNA-
564 seq datasets of COVID-19 patient lungs [58] showed that epithelial cells had the highest
565 *BTN3A2* expression (Fig. 1c), which are the primary target cells of SARS-CoV-2 [69].
566 We further explored *BTN3A2* expression patterns in NHPs challenged with
567 SARS-CoV-2, given their heightened resemblance to humans in the cellular identities
568 and frequencies of putative viral target cells [13, 70, 71]. Among 15 tissues tested in rhesus
569 monkeys [53], lung tissues showed the highest expression level of *BTN3A2*
570 (Supplementary Fig. S1c). Immunohistochemical analysis also showed that BTN3A2
571 was constitutively expressed in the healthy lung tissues of rhesus monkeys
572 (Supplementary Fig. S1d). We quantified the changes in *BTN3A2* mRNA expression
573 in rhesus and cynomolgus monkeys using qRT-PCR. Results indicated that *BTN3A2*
574 mRNA levels were significantly up-regulated in PBMCs and lung tissues at 7 dpi with
575 SARS-CoV-2 in rhesus macaques (Fig. 1d) and cynomolgus monkeys (Fig. 1e).
576 Similar *BTN3A2* mRNA expression patterns have also been observed in the
577 transcriptomic data of rhesus monkeys with early SARS-CoV-2 infection [53]
578 (Supplementary Fig. S1e). Collectively, these results indicated that *BTN3A2* is up-
579 regulated in COVID-19 patients and NHPs infected with SARS-CoV-2. In order to
580 determine whether the increased *BTN3A2* mRNA was caused by the induction of the
581 interferon system upon SARS-CoV-2 [5, 6], we treated Calu-3 cells with IFN-α, and

582 observed the up-regulation of full-length *BTN3A2* (*BTN3A2-L*) in cells treated with
583 IFN-α (Supplementary Fig. S1f).
584
585 **BTN3A2 acted as a potent SARS-CoV-2 restriction factor**
586 BTN3A2, a member of the immunoglobulin superfamily, is implicated in diverse
587 cellular processes [24]. BTN3A2 contains both full-length BTN3A2 (BTN3A2-L) and
588 truncated BTN3A2 (BTN3A2-S), as identified in our previous report [26]. To evaluate
589 the potential role of BTN3A2 in inhibiting SARS-CoV-2, we first ectopically
590 expressed the BTN3A family members (BTN3A1, BTN3A3, and BTN3A2) in ACE2-
591 A549 cells (Supplementary Fig. S2a), which were then infected with SARS-CoV-2.
592 Both BTN3A2 isoforms significantly inhibited SARS-CoV-2 viral copy numbers,
593 whereas BTN3A1 and BTN3A3 had no apparent inhibitory effect (Fig. 2a).
594 Compared to a higher multiplicity of infection (MOI), overexpression of BTN3A2 in
595 ACE2-HEK293T cells had a more potent inhibitory effect on lower infectious titers
596 (Fig. 2b and Supplementary Fig. S2b). The Huh7 cell line, which endogenously
597 expresses ACE2 and is naturally susceptible to SARS-CoV-2 [72], was used to validate
598 the above results. Overexpressing BTN3A2 in Huh7 cells (Supplementary Fig. S2c)
599 significantly reduced viral copies of the SARS-CoV-2 prototype and BA.2 variant in
600 cytoplasm and culture supernatant (Fig. 2c). Similar inhibitory effects were observed
601 using pseudotyped virus (which is a heterologous virus with Spike protein) [44] in
602 BTN3A2-L and BTN3A2-S Calu-3 cells (Fig. 2d). Interestingly, pre-incubation of
603 soluble BTN3A2-L and BTN3A2-S proteins in Calu-3 cells blocked viral entry into

604 cells, with a dose-dependent inhibitory effect (Fig. 2e).

605 To further test the potential role of endogenous BTN3A2 in controlling SARS-
606 CoV-2 infection, we depleted BTN3A2 expression in Huh7 cells using CRISPR-Cas9
607 gene editing, as described in our previous study [47], with two individual sgRNAs
608 (sgBTN3A2-1 and sgBTN3A2-3; Supplementary Fig. S2d). sgBTN3A2-1 and
609 sgBTN3A2-3 cells were more susceptible to authentic and pseudovirus SARS-CoV-2
610 than control sgNC cells (Fig. 2f-g). Thus, these findings suggest that BTN3A2 can
611 restrict SARS-CoV-2 infection.

612

613 **BTN3A2 directly interacted with Spike protein at RBD**

614 Next, we characterized the effects of BTN3A2 on specific steps of the viral
615 replication cycle. Initially, we assessed whether BTN3A2 inhibits SARS-CoV-2
616 attachment to the cell surface. Our data showed that SARS-CoV-2 viral copies were
617 significantly reduced in Huh7 cells with stable expression of BTN3A2-L and
618 BTN3A2-S, contrasting to corresponding control cells (Vector Huh7) (Fig. 3a and
619 Supplementary Fig. S3a). This result was confirmed by using a VSV-G pseudotyped
620 virus co-expressing SARS-CoV-2 spike protein and GFP reporter (VSV*ΔG-GFP
621 SARS-CoV-2 S) [42]. As expected, Huh7 cells overexpressing BTN3A2-L or BTN3A2-
622 S significantly inhibited VSV*ΔG-GFP SARS-CoV-2 S, whereas knockout of
623 BTN3A2 in Huh7 cells (sgBTN3A2-1 Huh7 cells and sgBTN3A2-3 Huh7 cells)
624 enhanced VSV*ΔG-GFP SARS-CoV-2 S replication (Supplementary Figs. S3b and
625 S3c). We performed a syncytia formation assay to test whether BTN3A2 restricts viral

626 entry using Huh7 cells overexpressing BTN3A2-L or BTN3A2-S. We found that
627 overexpression of BTN3A2-L and BTN3A2-S had no apparent effect on Spike
628 protein-mediated syncytia formation (Fig. 3b). These results suggested that BTN3A2
629 most likely interrupted the attachment step of viral invasion.

630 To assess whether BTN3A2 interacts with the SARS-CoV-2 Spike protein, an
631 envelope protein essential for host cell binding and entry[14, 15, 73], we conducted a co-
632 immunoprecipitation assay. Both BTN3A2 isoforms were co-immunoprecipitated
633 with the Spike protein in HEK293T cells (Fig. 3c). Given the reliance of not only
634 SARS-CoV-2 but also SARS-CoV [74] and HCoV-NL63 [75] on Spike protein-ACE2
635 interaction for cell entry, we examined whether BTN3A2 has a similar interaction
636 with the Spike proteins of SARS-CoV and HCoV-NL63. We observed an expected
637 interaction between BTN3A2 and Spike protein of SARS-CoV or HCoV-NL63
638 (Supplementary Fig. S3d), suggesting a potentially expanded role of BTN3A2 in the
639 related virus infections. Of note, BTN3A2-L interacted with the Spike S1 subunit but
640 not the S2 subunit (Fig. 3d), as further confirmed by the observation that endogenous
641 BTN3A2-L was immunoprecipitated by exogenous Spike S1 overexpression (Fig. 3e)
642 and the biolayer interferometry analysis (KD=92.7±0.111 nM) (Fig. 3f). Similarly, we
643 observed an interaction between BTN3A2-S and S1 subunit (Fig. 3g-h).

644 Considering a high degree of sequence identity between the extracellular regions
645 of BTN3A2 and its family member (BTN3A1 or BTN3A3), we further tested the
646 potential interaction between BTN3A members with S1. We found that BTN3A1 and
647 BTN3A3 could also interact with S1, but with a lower binding affinity comparing to

648 that of the interaction between BTN3A2 and S1 (Supplementary Fig. S4a-b). We
649 speculated that the lack of the intracellular B30.2 domain of BTN3A2 (relative to
650 BTN3A1 or BTN3A3) might be responsible for its high binding affinity to S1.
651 The S1 subunit, which contains the RBD, is both an inducer of dominant
652 neutralizing antibodies (nAbs) in the host and a key antigenic target for vaccine
653 development [41, 76, 77]. Subsequent co-immunoprecipitation assays confirmed that
654 BTN3A2-L interacted with the Spike protein RBD from multiple SARS-CoV-2
655 variants, including α, γ, δ, BA.1, BA.2, BA.2.12, and BA.5 (Fig. 3i). Similarly,
656 BTN3A2-S could interact with RBD of BA.2 (Supplementary Fig. S3e). These
657 findings established BTN3A2 as a novel cellular binding partner for the SARS-CoV-2
658 Spike protein specifically at the RBD.
659
660 **BTN3A2 competed with ACE2 to bind to RBD**
661 Although several host receptors for SARS-CoV-2 have been identified, only ACE2
662 interacts with the Spike protein via the RBD [78]. Thus, we tested whether BTN3A2
663 isoforms interact with ACE2, thereby modulating ACE2 and Spike protein
664 interactions during viral entry and replication. Both exogenously overexpressed
665 BTN3A2-L (His-tagged) (Fig. 4a-b) and endogenous BTN3A2 could interact with
666 exogenously overexpressed ACE2 according to our co-immunoprecipitation analyses
667 (Fig. 4c). This interaction could be further confirmed by the biolayer interferometry
668 analysis, in which an affinity between BTN3A2-L and ACE2 (KD=92.7±0.359 nM)
669 (Fig. 4d) was observed, indicating a direct association between BTN3A2-L and

670 ACE2. Compared to the interaction between BTN3A2-L and ACE2, a lower affinity
671 was observed between BTN3A2-S and ACE2 (KD=190±0.305 nM) (Fig. 4e) and
672 between the other BTN3A family member (BTN3A1, Supplementary Fig. S4c;
673 BTN3A3, Supplementary Fig. S4d) and ACE2.
674 As both ACE2 and BTN3A2 interacted with the Spike protein via its RBD, we
675 further investigated whether BTN3A2 competes with ACE2 for Spike S1 subunit
676 binding. Based on competitive ELISA, the interaction between ACE2 and SARS-
677 CoV-2 Spike was measured in the presence of recombinant BTN3A2-L protein (Fig.
678 4f). Results showed that Spike-ACE2 binding was greatly diminished under
679 increasing BTN3A2-L concentrations in a dose-dependent manner (Fig. 4g). Co-
680 immunoprecipitation assays demonstrated a decrease in the expression levels of
681 S1and ACE2 under the ectopic expression of BTN3A2-L in HEK293T cells (Fig. 4h),
682 while was in general consistent with a previous report showing a degradation of
683 ACE2 by SARS-CoV-2 Spike protein [79] in whole cell lysate (WCL). These findings
684 suggest that BTN3A2 interacts with the Spike through RBD binding, and ACE2 and
685 BTN3A2 compete for binding to the Spike protein.
686
687 **BTN3A2 inhibited ACE2 expression**
688 We next explored the potential role of the interactions among BTN3A2, ACE2, and
689 Spike protein in the context of COVID-19 pathology. We first compared the tissue
690 distribution patterns of BTN3A2 and ACE2. Re-analyses of a large-cohort RNA-seq
691 dataset of GTEx human tissues [59] showed that *BTN3A2* mRNA expression exhibited a

692 reverse correlation with *ACE2* in the lungs and gastrointestinal tract (small intestine)
693 (Supplementary Fig. S5a), which are major targets of SARS-CoV-2 infection. A
694 similar pattern was also observed in lung tissues and cell lines with or without SARS-
695 CoV-2 infection [80] (Supplementary Fig. S5b). We further compared *BTN3A2* co-
696 expression pattern with *ACE2* in different lung cell types using scRNA-seq data from
697 COVID-19 patients [58]. Our results indicated that, following SARS-CoV-2 infection,
698 *ACE2* mRNA could be detected at a slightly increased level in the lung epithelial cells
699 of COVID-19 patients, but *BTN3A2* expression was substantially up-regulated in the
700 same cell type (Fig. 5a). This observation suggested that the upregulation of *BTN3A2*
701 and *ACE2* mRNA was possibly controlled by different signaling pathways, although
702 BTN3A2 could reduce ACE2 protein expression. Consistently, the SARS-CoV-2-
703 infected lung tissues of NHPs had a lower level of *ACE2* mRNA compared to that of
704 lung tissues from uninfected animals (Supplementary Fig. S5c).
705 To further determine whether BTN3A2 affects ACE2 expression, we assessed
706 whether stable expression of *BTN3A2* in Huh7 cells altered the expression of *ACE2*
707 mRNA. Our results indicated that *ACE2* mRNA expression was significantly
708 decreased in Huh7 cells with stable expression of BTN3A2-L (BTN3A2-L Huh7
709 cells) and BTN3A2-S (BTN3A2-S Huh7 cells) (Fig. 5b). Consistently, total ACE2
710 protein expression was markedly decreased in HEK293T cells overexpressing both
711 BTN3A2-L and ACE2 compared to cells overexpressing ACE2 only (Fig. 5c).
712 However, BTN3A2-S had minor effect on inhibiting ACE2 expression in HEK293T
713 cells (Fig. 5d) compared to BTN3A2-L. The inhibitory effects of BTN3A2-L on

714 ACE2 expression were dose-dependent (Fig. 5e). Knockout of BTN3A2 in Huh7 cells
715 (sgBTN3A2-1 Huh7 cells and sgBTN3A2-3 Huh7 cells) led to a significant increase
716 in both *ACE2* mRNA (Fig. 5f) and protein levels (Fig. 5g). Using flow cytometry, we
717 further assessed whether BTN3A2 alters ACE2 expression on the cell surface.
718 Notably, ACE2 expression on the cell surface was significantly decreased in Calu-3
719 cells with stable expression of BTN3A2-L (BTN3A2-L Calu-3 cells) and BTN3A2-S
720 (BTN3A2-S Calu-3 cells), while knockout of BTN3A2 in Calu-3 cells (sgBTN3A2-1
721 Calu-3 cells and sgBTN3A2-3 Calu-3 cells) increased the surface level of ACE2 (Fig.
722 5h-i). Similar results were observed in genetic modified Huh7 cell lines
723 (Supplementary Fig. S5d-e), indicating that BTN3A2 inhibits ACE2 expression *in*
724 *vitro*.
725 As *BTN3A2* is a primate-specific gene [26], we used BTN3A2-tg mice to further
726 characterize the level of ACE2 *in vivo*. WT C57BL/6J mice were used as a control.
727 Mice were intranasally infected with AAV-hACE2 (AAV carrying the human *ACE2*
728 gene, AAV-hACE2 group) or AAV-EGFP (AAV-EGFP group, control group).
729 Immunoblot analysis showed that EGFP levels were similar between the BTN3A2-tg
730 and WT C57BL/6J mice (WT control) (Fig. 5j), indicating effective viral vector-
731 mediated gene expression. Consistent with the cellular assays and inhibitory effects of
732 BTN3A2 on ACE2 expression, our results further showed that the ACE2 protein level
733 was significantly lower in BTN3A2-tg mice relative to WT C57BL/6J mice (Fig. 5j).
734 The AAV vectors achieved efficient EGFP and ACE2 expression in the lung tissues of
735 WT mice at 14 dpi with AAV (Fig. 5k and Supplementary Fig. S5f). Conversely,

736 ACE2 was barely detected in the lung tissues of BTN3A2-tg mice (Fig. 5k and
737 Supplementary Fig. S5f). Collectively, these results suggest that BTN3A2 suppression
738 of ACE2 also occurs *in vivo*.
739
740 **BTN3A2 suppressed SARS-CoV-2 infection by reducing ACE2**
741 We further evaluated whether the suppression of ACE2 expression by BTN3A2 is
742 responsible for BTN3A2-mediated SARS-CoV-2 restriction. We intranasally injected
743 AAV9-hACE2 in WT C57BL/6J and BTN3A2 transgenic (BTN3A2-tg) heterozygous
744 mice and observed for two weeks, followed by SARS-CoV-2 challenge and sacrifice
745 for tissue collection at 3 dpi (Fig. 6a). Quantitative analysis of viral loads, specifically
746 targeting the nucleoprotein gene (*N*) and envelope gene (*E*), revealed a 3-fold to 6-
747 fold decrease in lung tissue viral concentrations in BTN3A2-tg mice compared to
748 their WT counterparts (Fig. 6b). Of the seven infected WT C57BL/6J mice examined,
749 five exhibited detectable levels of viral subgenomic RNA in their lung tissues,
750 including the subgenomic E (sgE) gene, a marker of infectious virus [38, 81]. In contrast,
751 none of the six BTN3A2-tg mice showed detectable levels of sgE gene. Further
752 immunohistochemical staining of the SARS-CoV-2 nucleoprotein (N) showed a
753 consistent reduction in viral protein levels in the lung tissues of BTN3A2-tg mice
754 compared to the infected WT C57BL/6J mice (Fig. 6c). Moreover, histological
755 analysis showed that the lung tissues of the SARS-CoV-2 infected BTN3A2-tg mice
756 had milder damage, including the widening, fusion, and increased solidity of the
757 pulmonary septa, compared to the infected WT C57BL/6J mice (Fig. 6d), suggesting a

758 protective role of BTN3A2 in counteracting SARS-CoV-2 infection. Similarly, we
759 observed consistent and effective expression of hACE2 in the lung tissues of the WT
760 group, while the protein level of ACE2 was greatly reduced in the lung tissues of the
761 BTN3A2-tg mice, as expected (Fig. 6e). This pattern was further validated by
762 immunohistochemical analysis of lung tissues from both groups: ACE2 was
763 consistently and highly expressed in the upper and lower respiratory tract of WT mice
764 (Fig. 6f) but was barely detected in the respiratory tract of BTN3A2-tg mice.
765 Collectively, these results suggest that BTN3A2 can restrict SARS-CoV-2 by
766 suppressing ACE2-mediated viral entry *in vivo*.
767
768 **Discussion**
769
770 Understanding the pathobiology of SARS-CoV-2 infection is essential for developing
771 effective treatments. Various studies have examined the host immune response in
772 relation to SARS-CoV-2 infection [50, 82, 83]. Specifically, the balanced regulation of
773 interferon signaling and immune response has been shown to substantially influence
774 disease severity and outcomes of COVID-19 [6, 84]. In the current study, we identified
775 BTN3A2 as a novel factor involved in the defense against SARS-CoV-2 infection.
776 Notably, BTN3A2 was up-regulated upon SARS-CoV-2 infection and directly
777 interacted with the RBD of the Spike protein. This interaction was confirmed through
778 both cell-free binding assays utilizing recombinant proteins and co-
779 immunoprecipitation assays conducted in cellular environments. This led to

780 competitive interference with the interaction between ACE2 and the RBD of the Spike
781 protein, as reported previously [13, 85]. Given that BTN3A2 is a single transmembrane
782 protein localized to the cellular membrane [86], it is plausible that a complex between
783 BTN3A2 and the Spike protein may effectively obstruct the binding of the Spike
784 protein to ACE2 on the cellular surface. Remarkably, BTN3A2-S, which lacks a
785 transmembrane domain, demonstrated greater efficacy than BTN3A2-L in inhibiting
786 the attachment of the Spike protein to the cellular surface, thereby reducing SARS-
787 CoV-2 infection. We hypothesize that secreted BTN3A2-S [26] may possess enhanced
788 inhibitory effects against SARS-CoV-2 Spike binding to ACE2, akin to the function of
789 neutralizing antibodies. Investigating the structural characteristics and molecular
790 dynamics of the BTN3A2-Spike protein complex could offer substantial insights for
791 the engineering of short peptides that retain the full competitive capacity of BTN3A2
792 in challenging ACE2 for Spike protein binding.

793 Reducing ACE2 expression has been considered a potentially efficacious host-
794 directed prophylaxis for protection against SARS-CoV-2 infection [23, 83]. Beyond the
795 competitive effects of BTN3A2 on ACE2-Spike binding, our study demonstrated that
796 BTN3A2 interacted with ACE2, leading to a further decrease in ACE2 expression.
797 Overexpression of BTN3A2 led to a reduction in *ACE2* mRNA and protein levels,
798 which further inhibited ACE2-mediated SARS-CoV-2 infection, both *in vitro* and *in*
799 *vivo*. While the exact mechanism by which BTN3A2 regulates ACE2 expression
800 remains to be determined, the apparent dual role of BTN3A2 in regulating ACE2
801 expression and function is consistent with the concept that targeting universal host

802 factors essential for viral replication offers advantages in terms of broad-spectrum
803 effectiveness and reduced drug resistance [87, 88].
804 The ongoing COVID-19 pandemic, coupled with the emergence of new SARS-
805 CoV-2 variants, necessitates the development of novel broad-spectrum vaccines and
806 antiviral therapies. Recent studies have identified several potential targets for SARS-
807 CoV-2 intervention, including the transcriptional regulator BRD2 [83], aryl hydrocarbon
808 receptor (AhR) [8], and host cysteine-aspartic protease caspase-6 [89], for which specific
809 compounds have been characterized. Given the observed protective effects of
810 BTN3A2 against SARS-CoV-2 infection, we speculate that BTN3A2 may be a viable
811 host factor candidate with broad antiviral potential. Indeed, pre-incubation of soluble
812 BTN3A2 protein with host cells resulted in decreased viral entry. Notably,
813 interactions between BTN3A2 and the Spike protein RBD of various SARS-CoV-2
814 variants of concern (VOCs) (e.g., prototype, α, γ, δ, and omicron) remained largely
815 stable despite the rich diversity and evolution of viral sequences. These findings
816 suggest the anti-coronavirus activity of BTN3A2 may be both conserved and
817 efficacious across multiple SARS-CoV-2 VOCs.
818 The primate-specific *BTN3A2* gene [26] is highly expressed in the brain. Thus, it
819 may have a role in the development of long COVID and brain fog, conditions
820 characterized by a multitude of persistent neurological symptoms that last for months
821 after SARS-CoV-2 infection [90]. Currently, the pathophysiological mechanisms
822 associated with neurological symptoms derived from SARS-CoV-2 infection remain
823 to be elucidated [91]. We recently showed that the S2 subunit of the SARS-CoV-2 Spike

824 protein modulates γ-secretase and enhances Aβ production, which may contribute to
825 the neurological alterations observed in COVID-19 patients [45]. Respiratory infection
826 with SARS-CoV-2 can elicit neuroinflammation and dysfunction in neural cells and
827 myelin [92]. Modulation of the immune environment within the central nervous system,
828 particularly in scenarios where neuroinflammation is triggered by inflammation in the
829 respiratory system, may influence the neuroprotective and neuroplastic functions of
830 specific immune cell populations, including γδ T cells [93], following COVID-19 [91].
831 Therefore, given the broad immune cell expression of BTN3A2 and its involvement
832 in γδ T cell regulation [27, 94], determining the roles of BTN3A2 in T cell-mediated
833 immune responses, neuroinflammation, and long COVID-19 would be worthwhile.
834 This study has several limitations. Firstly, although we presented multiple lines of
835 evidence to show the active role of BTN3A2 as a key host factor in combating SARS-
836 CoV-2 infection, how BTN3A2 was upregulated upon SARS-CoV-2 infection, and
837 which signaling pathways were activated in this process remain unknown. It could be
838 possible that induction of the interferon system by SARS-CoV-2 led to an increased
839 expression of *BTN3A2*, as shown by the fact that the *BTN3A2* expression was
840 upregulated in IFN-α treated Calu-3 cells (Supplementary Fig. S1f) and Huh7 cells
841 (Fig. 3e and Fig. 4c). Focused study should be performed to refine this mechanism.
842 Secondly, we showed evidence that BTN3A2 interacts with the Spike proteins of
843 SARS-CoV-2 VOCs, indicating a potential broad-spectrum antiviral role of BTN3A2.
844 This speculation deserves further validations. Thirdly, as a single-pass transmembrane
845 protein on the host cell membrane, whether BTN3A2, by competitively binding to the

RBD of the Spike protein, could function as an alternative receptor for SARS-CoV-2 and assist in viral invasion, is an arising question from this study.

In conclusion, we identified BTN3A2 as a novel host factor with protective effects against SARS-CoV-2 infection. Thus, BTN3A2 holds considerable potential as a therapeutic drug for mitigating the impact of SARS-CoV-2 VOCs. However, subsequent research is warranted to explore its potential role in the occurrence of neurological symptoms, commonly referred to as “brain fog”, in COVID-19 patients.

Contributors

L.X., N.S., Y.-G.Y. conceptualized the study. L.X., D.Y., M.X., Y.L., L.-X.Y., Q-C.Z., X.-L.F., M.-H.L. performed the experiments. D.Y., L.-X.Y., Q-C.Z. verified the underlying data, L.X., D.Y. and M.X. analyzed the data. L.X., D.Y., M.X., Y.-G.Y. wrote the manuscript. Y.-G.Y. and N.S. supervised the study and revised the manuscript. All authors have given approval to the final version of the manuscript.

Data Sharing Statement

Data reported in this paper will be shared by the lead contact upon reasonable request. This paper does not report original code.

Declaration of interests

The authors declare that they have no competing interests.

Acknowledgments

We thank Drs. Yu-Lin Yao and Yong Wu for technical discussions. We are grateful to Profs. Qihui Wang and Yong-Tang Zheng for sharing the VSV-G pseudotyped viruses.

References

1. Wiersinga WJ, Rhodes A, Cheng AC, Peacock SJ, Prescott HC. Pathophysiology, transmission, diagnosis, and treatment of coronavirus disease 2019 (COVID-19): a review. *JAMA* 2020; **324** (8):782-793.
2. Mehandru S, Merad M. Pathological sequelae of long-haul COVID. *Nat Immunol* 2022; **23** (2):194-202.
3. Organization WH. Coronavirus disease (COVID-19) pandemic. *World Health Organization* 2023.
4. Parotto M, Gyöngyösi M, Howe K, Myatra SN, Ranzani O, Shankar-Hari M *et al.* Post-acute sequelae of COVID-19: understanding and addressing the burden of multisystem manifestations. *Lancet Respir Med* 2023; **11** (8):739-754.
5. Minkoff JM, tenOever B. Innate immune evasion strategies of SARS-CoV-2. *Nat Rev Microbiol* 2023; **21** (3):178-194.
6. Sievers BL, Cheng MTK, Csiba K, Meng B, Gupta RK. SARS-CoV-2 and innate immunity: the good, the bad, and the "goldilocks". *Cell Mol Immunol* 2024; **21** (2):171-183.
7. Barouch DH. Covid-19 vaccines - immunity, variants, boosters. *N Engl J Med* 2022; **387** (11):1011-1020.

890 8. Shi J, Du T, Wang J, Tang C, Lei M, Yu W *et al.* Aryl hydrocarbon receptor is a
891 proviral host factor and a candidate pan-SARS-CoV-2 therapeutic target. *Sci Adv*
892 2023; **9** (22):eadf0211.
893 9. Li G, Hilgenfeld R, Whitley R, De Clercq E. Therapeutic strategies for COVID-19:
894 progress and lessons learned. *Nat Rev Drug Discov* 2023; **22** (6):449-475.
895 10. Teijaro JR, Farber DL. COVID-19 vaccines: modes of immune activation and
896 future challenges. *Nat Rev Immunol* 2021; **21** (4):195-197.
897 11. Lu G, Wang Q, Gao GF. Bat-to-human: spike features determining 'host jump' of
898 coronaviruses SARS-CoV, MERS-CoV, and beyond. *Trends Microbiol* 2015; **23**
899 (8):468-478.
900 12. Zhao R, Niu S, Han P, Gao Y, Liu D, Luo C *et al.* Cross-species recognition of bat
901 coronavirus RsYN04 and cross-reaction of SARS-CoV-2 antibodies against the
902 virus. *Zool Res* 2023; **44** (6):1015-1025.
903 13. Ziegler CGK, Allon SJ, Nyquist SK, Mbano IM, Miao VN, Tzouanas CN *et al.*
904 SARS-CoV-2 receptor ACE2 is an interferon-stimulated gene in human airway
905 epithelial cells and is detected in specific cell subsets across tissues. *Cell* 2020; **181**
906 (5):1016-1035.e1019.
907 14. Taft JM, Weber CR, Gao B, Ehling RA, Han J, Frei L *et al.* Deep mutational
908 learning predicts ACE2 binding and antibody escape to combinatorial mutations in
909 the SARS-CoV-2 receptor-binding domain. *Cell* 2022; **185** (21):4008-4022.e4014.
910 15. Zhou P, Yang XL, Wang XG, Hu B, Zhang L, Zhang W *et al.* A pneumonia outbreak
911 associated with a new coronavirus of probable bat origin. *Nature* 2020; **579**

912 (7798):270-273.

913 16. Li Q, Wu J, Nie J, Zhang L, Hao H, Liu S *et al.* The impact of mutations in SARS-
914 CoV-2 spike on viral infectivity and antigenicity. *Cell* 2020; **182** (5):1284-
915 1294.e1289.

916 17. Wu L, Chen Q, Liu K, Wang J, Han P, Zhang Y *et al.* Broad host range of SARS-
917 CoV-2 and the molecular basis for SARS-CoV-2 binding to cat ACE2. *Cell Discov*
918 2020; **6**:68.

919 18. Chen DY, Chin CV, Kenney D, Tavares AH, Khan N, Conway HL *et al.* Spike and
920 nsp6 are key determinants of SARS-CoV-2 Omicron BA.1 attenuation. *Nature*
921 2023; **615** (7950):143-150.

922 19. Dadonaite B, Crawford KHD, Radford CE, Farrell AG, Yu TC, Hannon WW *et al.*
923 A pseudovirus system enables deep mutational scanning of the full SARS-CoV-2
924 spike. *Cell* 2023; **186** (6):1263-1278.e1220.

925 20. Chen C, Wang X, Zhang Z. Humoral and cellular immunity against diverse SARS-
926 CoV-2 variants. *J Genet Genomics* 2023; **50** (12):934-947.

927 21. Gaziano L, Giambartolomei C, Pereira AC, Gaulton A, Posner DC, Swanson SA
928 *et al.* Actionable druggable genome-wide Mendelian randomization identifies
929 repurposing opportunities for COVID-19. *Nat Med* 2021; **27** (4):668-676.

930 22. Shu CJ, Huang X, Tang HH, Mo DD, Zhou JW, Deng C. Mutations in spike protein
931 and allele variations in ACE2 impact targeted therapy strategies against SARS-
932 CoV-2. *Zool Res* 2021; **42** (2):170-181.

933 23. Brevini T, Maes M, Webb GJ, John BV, Fuchs CD, Buescher G *et al.* FXR

934 inhibition may protect from SARS-CoV-2 infection by reducing ACE2. *Nature*
935 2023; **615** (7950):134-142.
936 24. Afrache H, Gouret P, Ainouche S, Pontarotti P, Olive D. The butyrophilin (BTN)
937 gene family: from milk fat to the regulation of the immune response.
938 *Immunogenetics* 2012; **64** (11):781-794.
939 25. Tazi-Ahnini R, Henry J, Offer C, Bouissou-Bouchouata C, Mather IH, Pontarotti
940 P. Cloning, localization, and structure of new members of the butyrophilin gene
941 family in the juxta-telomeric region of the major histocompatibility complex.
942 *Immunogenetics* 1997; **47** (1):55-63.
943 26. Wu Y, Bi R, Zeng C, Ma C, Sun C, Li J *et al.* Identification of the primate-specific
944 gene BTN3A2 as an additional schizophrenia risk gene in the MHC loci.
945 *EBioMedicine* 2019; **44**:530-541.
946 27. Arnett HA, Viney JL. Immune modulation by butyrophilins. *Nat Rev Immunol*
947 2014; **14** (8):559-569.
948 28. Yuan L, Ma X, Yang Y, Qu Y, Li X, Zhu X *et al.* Phosphoantigens glue butyrophilin
949 3A1 and 2A1 to activate Vγ9Vδ2 T cells. *Nature* 2023; **621** (7980):840-848.
950 29. Payne KK, Mine JA, Biswas S, Chaurio RA, Perales-Puchalt A, Anadon CM *et al.*
951 BTN3A1 governs antitumor responses by coordinating αβ and γδ T cells. *Science*
952 2020; **369** (6506):942-949.
953 30. Karunakaran MM, Willcox CR, Salim M, Paletta D, Fichtner AS, Noll A *et al.*
954 Butyrophilin-2A1 directly binds germline-encoded regions of the Vγ9Vδ2 TCR
955 and is essential for phosphoantigen sensing. *Immunity* 2020; **52** (3):487-498.e486.

956 31. de Groot N, Groen R, Orie V, Bruijnesteijn J, de Groot NG, Doxiadis GGM *et al.*
957 Analysis of macaque BTN3A genes and transcripts in the extended MHC:
958 conserved orthologs of human γδ T cell modulators. *Immunogenetics* 2019; **71** (8-
959 9):545-559.
960 32. Yang H, Liu D, Zhao C, Feng B, Lu W, Yang X *et al.* Mendelian randomization
961 integrating GWAS and eQTL data revealed genes pleiotropically associated with
962 major depressive disorder. *Transl Psychiatry* 2021; **11** (1):225.
963 33. Li J, Yoshikawa A, Alliey-Rodriguez N, Meltzer HY. Schizophrenia risk loci from
964 xMHC region were associated with antipsychotic response in chronic
965 schizophrenic patients with persistent positive symptom. *Transl Psychiatry* 2022;
966 **12** (1):92.
967 34. Li H, Chang H, Song X, Liu W, Li L, Wang L *et al.* Integrative analyses of major
968 histocompatibility complex loci in the genome-wide association studies of major
969 depressive disorder. *Neuropsychopharmacology* 2019; **44** (9):1552-1561.
970 35. Kuroda M, Halfmann PJ, Hill-Batorski L, Ozawa M, Lopes TJS, Neumann G *et al.*
971 Identification of interferon-stimulated genes that attenuate Ebola virus infection.
972 *Nat Commun* 2020; **11** (1):2953.
973 36. Pinto RM, Bakshi S, Lytras S, Zakaria MK, Swingler S, Worrell JC *et al.* BTN3A3
974 evasion promotes the zoonotic potential of influenza A viruses. *Nature* 2023; **619**
975 (7969):338-347.
976 37. Xu L, Yu DD, Ma YH, Yao YL, Luo RH, Feng XL *et al.* COVID-19-like symptoms
977 observed in Chinese tree shrews infected with SARS-CoV-2. *Zool Res* 2020; **41**

978 (5):517-526.

979 38. Yu D, Long Y, Xu L, Han JB, Xi J, Xu J *et al.* Infectivity of SARS-CoV-2 and
980 protection against reinfection in rats. *Zool Res* 2022; **43** (6):945-948.

981 39. Feng XL, Yu D, Zhang M, Li X, Zou QC, Ma W *et al.* Characteristics of replication
982 and pathogenicity of SARS-CoV-2 Alpha and Delta isolates. *Virol Sin* 2022; **37**
983 (6):804-812.

984 40. Zheng HY, Xu M, Yang CX, Tian RR, Zhang M, Li JJ *et al.* Longitudinal
985 transcriptome analyses show robust T cell immunity during recovery from COVID-
986 19. *Signal Transduct Target Ther* 2020; **5** (1):294.

987 41. Shi R, Zeng J, Xu L, Wang F, Duan X, Wang Y *et al.* A combination vaccine against
988 SARS-CoV-2 and H1N1 influenza based on receptor binding domain trimerized
989 by six-helix bundle fusion core. *EBioMedicine* 2022; **85**:104297.

990 42. Wu L, Gao Y, Yu D, Liu S, Zhao R, Liu D *et al.* VH-CH1 switch region-inserting
991 multispecific antibody designs and their efficacy against SARS-CoV-2 in vitro and
992 in vivo. *Cell Discov* 2023; **9** (1):113.

993 43. Li M, Ferretti M, Ying B, Descamps H, Lee E, Dittmar M *et al.* Pharmacological
994 activation of STING blocks SARS-CoV-2 infection. *Sci Immunol* 2021; **6**
995 (59):eabi9007.

996 44. Pang W, Lu Y, Zhao YB, Shen F, Fan CF, Wang Q *et al.* A variant-proof SARS-
997 CoV-2 vaccine targeting HR1 domain in S2 subunit of spike protein. *Cell Res* 2022;
998 **32** (12):1068-1085.

999 45. Ma G, Zhang DF, Zou QC, Xie X, Xu L, Feng XL *et al.* SARS-CoV-2 Spike protein

1000 S2 subunit modulates γ-secretase and enhances amyloid-β production in COVID-
1001 19 neuropathy. *Cell Discov* 2022; **8** (1):99.
1002 46. Xu L, Yu D, Fan Y, Peng L, Wu Y, Yao YG. Loss of RIG-I leads to a functional
1003 replacement with MDA5 in the Chinese tree shrew. *Proc Natl Acad Sci U S A* 2016;
1004 **113** (39):10950-10955.
1005 47. Xu L, Yu D, Yao YL, Gu T, Zheng X, Wu Y *et al. Tupaia* MAVS is a dual target
1006 during Hepatitis C virus infection for innate immune evasion and viral replication
1007 via NF-κB. *J Immunol* 2020; **205** (8):2091-2099.
1008 48. Zeng J, Xie X, Feng XL, Xu L, Han JB, Yu D *et al.* Specific inhibition of the
1009 NLRP3 inflammasome suppresses immune overactivation and alleviates COVID-
1010 19 like pathology in mice. *EBioMedicine* 2022; **75**:103803.
1011 49. Bolland W, Michel V, Planas D, Hubert M, Staropoli I, Guivel-Benhassine F *et al.*
1012 High fusion and cytopathy of SARS-CoV-2 variant B.1.640.1. *J Virol* 2024; **98**
1013 (1):e0135123.
1014 50. Pfaender S, Mar KB, Michailidis E, Kratzel A, Boys IN, V'Kovski P *et al.* LY6E
1015 impairs coronavirus fusion and confers immune control of viral disease. *Nat*
1016 *Microbiol* 2020; **5** (11):1330-1339.
1017 51. Overmyer KA, Shishkova E, Miller IJ, Balnis J, Bernstein MN, Peters-Clarke TM
1018 *et al.* Large-Scale Multi-omic Analysis of COVID-19 Severity. *Cell Syst* 2021; **12**
1019 (1):23-40.e27.
1020 52. Dean MJ, Ochoa JB, Sanchez-Pino MD, Zabaleta J, Garai J, Del Valle L *et al.*
1021 Severe COVID-19 Is characterized by an impaired type I interferon response and

1022 elevated levels of arginase producing granulocytic myeloid derived suppressor
1023 cells. *Front Immunol* 2021; **12**:695972.
1024 53. Gao CC, Li M, Deng W, Ma CH, Chen YS, Sun YQ *et al.* Differential
1025 transcriptomic landscapes of multiple organs from SARS-CoV-2 early infected
1026 rhesus macaques. *Protein Cell* 2022; **13** (12):920-939.
1027 54. Bolger AM, Lohse M, Usadel B. Trimmomatic: a flexible trimmer for Illumina
1028 sequence data. *Bioinformatics* 2014; **30** (15):2114-2120.
1029 55. Dobin A, Davis CA, Schlesinger F, Drenkow J, Zaleski C, Jha S *et al.* STAR:
1030 ultrafast universal RNA-seq aligner. *Bioinformatics* 2013; **29** (1):15-21.
1031 56. Li B, Dewey CN. RSEM: accurate transcript quantification from RNA-Seq data
1032 with or without a reference genome. *BMC Bioinformatics* 2011; **12**:323.
1033 57. Tian Y, Carpp LN, Miller HER, Zager M, Newell EW, Gottardo R. Single-cell
1034 immunology of SARS-CoV-2 infection. *Nat Biotechnol* 2022; **40** (1):30-41.
1035 58. Melms JC, Biermann J, Huang H, Wang Y, Nair A, Tagore S *et al.* A molecular
1036 single-cell lung atlas of lethal COVID-19. *Nature* 2021; **595** (7865):114-119.
1037 59. Consortium G. The Genotype-Tissue Expression (GTEx) project. *Nat Genet* 2013;
1038 **45** (6):580-585.
1039 60. Eraslan G, Drokhlyansky E, Anand S, Fiskin E, Subramanian A, Slyper M *et al.*
1040 Single-nucleus cross-tissue molecular reference maps toward understanding
1041 disease gene function. *Science* 2022; **376** (6594):eabl4290.
1042 61. Blanco-Melo D, Nilsson-Payant BE, Liu WC, Uhl S, Hoagland D, Møller R *et al.*
1043 Imbalanced host response to SARS-CoV-2 drives development of COVID-19. *Cell*

1044 2020; **181** (5):1036-1045.e1039.

1045 62. Daamen AR, Bachali P, Owen KA, Kingsmore KM, Hubbard EL, Labonte AC *et*
1046 *al.* Comprehensive transcriptomic analysis of COVID-19 blood, lung, and airway.
1047 *Sci Rep* 2021; **11** (1):7052.

1048 63. Love MI, Huber W, Anders S. Moderated estimation of fold change and dispersion
1049 for RNA-seq data with DESeq2. *Genome Biol* 2014; **15** (12):550.

1050 64. Ritchie ME, Phipson B, Wu D, Hu Y, Law CW, Shi W *et al.* limma powers
1051 differential expression analyses for RNA-sequencing and microarray studies.
1052 *Nucleic Acids Res* 2015; **43** (7):e47.

1053 65. Sun S, Cai Y, Song TZ, Pu Y, Cheng L, Xu H *et al.* Interferon-armed RBD dimer
1054 enhances the immunogenicity of RBD for sterilizing immunity against SARS-
1055 CoV-2. *Cell Res* 2021; **31** (9):1011-1023.

1056 66. Liu Y, Dai L, Feng X, Gao R, Zhang N, Wang B *et al.* Fast and long-lasting immune
1057 response to S-trimer COVID-19 vaccine adjuvanted by PIKA. *Mol Biomed* 2021;
1058 **2** (1):29.

1059 67. Bost P, De Sanctis F, Canè S, Ugel S, Donadello K, Castellucci M *et al.*
1060 Deciphering the state of immune silence in fatal COVID-19 patients. *Nat Commun*
1061 2021; **12** (1):1428.

1062 68. Yamashiro H, Yoshizaki S, Tadaki T, Egawa K, Seo N. Stimulation of human
1063 butyrophilin 3 molecules results in negative regulation of cellular immunity. *J*
1064 *Leukoc Biol* 2010; **88** (4):757-767.

1065 69. Delorey TM, Ziegler CGK, Heimberg G, Normand R, Yang Y, Segerstolpe Å *et al.*

1066 COVID-19 tissue atlases reveal SARS-CoV-2 pathology and cellular targets.
1067 *Nature* 2021; **595** (7865):107-113.
1068 70. Ma Q, Ma W, Song TZ, Wu Z, Liu Z, Hu Z *et al.* Single-nucleus transcriptomic
1069 profiling of multiple organs in a rhesus macaque model of SARS-CoV-2 infection.
1070 *Zool Res* 2022; **43** (6):1041-1062.
1071 71. Zhang X, Lai GY, Volpe G, Han L, Maxwell PH, Liu LQ *et al.* Towards a primate
1072 single-cell atlas. *Zool Res* 2022; **43** (4):691-694.
1073 72. Harcourt J, Tamin A, Lu X, Kamili S, Sakthivel SK, Murray J *et al.* Severe acute
1074 respiratory syndrome coronavirus 2 from patient with coronavirus disease, United
1075 States. *Emerg Infect Dis* 2020; **26** (6):1266-1273.
1076 73. Shang J, Wan Y, Luo C, Ye G, Geng Q, Auerbach A *et al.* Cell entry mechanisms
1077 of SARS-CoV-2. *Proc Natl Acad Sci U S A* 2020; **117** (21):11727-11734.
1078 74. Li W, Moore MJ, Vasilieva N, Sui J, Wong SK, Berne MA *et al.* Angiotensin-
1079 converting enzyme 2 is a functional receptor for the SARS coronavirus. *Nature*
1080 2003; **426** (6965):450-454.
1081 75. Hofmann H, Pyrc K, van der Hoek L, Geier M, Berkhout B, Pöhlmann S. Human
1082 coronavirus NL63 employs the severe acute respiratory syndrome coronavirus
1083 receptor for cellular entry. *Proc Natl Acad Sci U S A* 2005; **102** (22):7988-7993.
1084 76. Liu L, Wang P, Nair MS, Yu J, Rapp M, Wang Q *et al.* Potent neutralizing
1085 antibodies against multiple epitopes on SARS-CoV-2 spike. *Nature* 2020; **584**
1086 (7821):450-456.
1087 77. Piccoli L, Park YJ, Tortorici MA, Czudnochowski N, Walls AC, Beltramello M *et*

1088 *al.* Mapping neutralizing and immunodominant sites on the SARS-CoV-2 spike
1089 receptor-binding domain by structure-guided high-resolution serology. *Cell* 2020;
1090 **183** (4):1024-1042.e1021.
1091 78. Lan J, Ge J, Yu J, Shan S, Zhou H, Fan S *et al.* Structure of the SARS-CoV-2 spike
1092 receptor-binding domain bound to the ACE2 receptor. *Nature* 2020; **581**
1093 (7807):215-220.
1094 79. Gao X, Zhang S, Gou J, Wen Y, Fan L, Zhou J *et al.* Spike-mediated ACE2 down-
1095 regulation was involved in the pathogenesis of SARS-CoV-2 infection. *J Infect*
1096 2022; **85** (4):418-427.
1097 80. Sun X, Liu Y, Huang Z, Xu W, Hu W, Yi L *et al.* SARS-CoV-2 non-structural
1098 protein 6 triggers NLRP3-dependent pyroptosis by targeting ATP6AP1. *Cell Death*
1099 *Differ* 2022; **29** (6):1240-1254.
1100 81. Dagotto G, Mercado NB, Martinez DR, Hou YJ, Nkolola JP, Carnahan RH *et al.*
1101 Comparison of subgenomic and total RNA in SARS-CoV-2 challenged rhesus
1102 macaques. *J Virol* 2021; **95** (8):e02370-02320.
1103 82. Xu D, Jiang W, Wu L, Gaudet RG, Park ES, Su M *et al.* PLSCR1 is a cell-
1104 autonomous defence factor against SARS-CoV-2 infection. *Nature* 2023; **619**
1105 (7971):819-827.
1106 83. Samelson AJ, Tran QD, Robinot R, Carrau L, Rezelj VV, Kain AM *et al.* BRD2
1107 inhibition blocks SARS-CoV-2 infection by reducing transcription of the host cell
1108 receptor ACE2. *Nat Cell Biol* 2022; **24** (1):24-34.
1109 84. Hadjadj J, Yatim N, Barnabei L, Corneau A, Boussier J, Smith N *et al.* Impaired

1110 type I interferon activity and inflammatory responses in severe COVID-19 patients.
1111 *Science* 2020; **369** (6504):718-724.
1112 85. Damas J, Hughes GM, Keough KC, Painter CA, Persky NS, Corbo M *et al.* Broad
1113 host range of SARS-CoV-2 predicted by comparative and structural analysis of
1114 ACE2 in vertebrates. *Proc Natl Acad Sci U S A* 2020; **117** (36):22311-22322.
1115 86. Vantourout P, Laing A, Woodward MJ, Zlatareva I, Apolonia L, Jones AW *et al.*
1116 Heteromeric interactions regulate butyrophilin (BTN) and BTN-like molecules
1117 governing γδ T cell biology. *Proc Natl Acad Sci U S A* 2018; **115** (5):1039-1044.
1118 87. Zheng Y, Li S, Song K, Ye J, Li W, Zhong Y *et al.* A broad antiviral strategy:
1119 inhibitors of human DHODH pave the way for host-targeting antivirals against
1120 emerging and re-emerging viruses. *Viruses* 2022; **14** (5):928.
1121 88. Mahajan S, Choudhary S, Kumar P, Tomar S. Antiviral strategies targeting host
1122 factors and mechanisms obliging +ssRNA viral pathogens. *Bioorg Med Chem* 2021;
1123 **46**:116356.
1124 89. Chu H, Hou Y, Yang D, Wen L, Shuai H, Yoon C *et al.* Coronaviruses exploit a host
1125 cysteine-aspartic protease for replication. *Nature* 2022; **609** (7928):785-792.
1126 90. Nasserie T, Hittle M, Goodman SN. Assessment of the frequency and variety of
1127 persistent symptoms among patients With COVID-19: A systematic review. *JAMA*
1128 *Netw Open* 2021; **4** (5):e2111417.
1129 91. Monje M, Iwasaki A. The neurobiology of long COVID. *Neuron* 2022; **110**
1130 (21):3484-3496.
1131 92. Fernández-Castañeda A, Lu P, Geraghty AC, Song E, Lee MH, Wood J *et al.* Mild

1132 respiratory COVID can cause multi-lineage neural cell and myelin dysregulation.
1133 *Cell* 2022; **185** (14):2452-2468.e2416.
1134 93. Ribeiro M, Brigas HC, Temido-Ferreira M, Pousinha PA, Regen T, Santa C *et al.*
1135 Meningeal γδ T cell-derived IL-17 controls synaptic plasticity and short-term
1136 memory. *Sci Immunol* 2019; **4** (40):eaay5199.
1137 94. Gu S, Borowska MT, Boughter CT, Adams EJ. Butyrophilin3A proteins and
1138 Vγ9Vδ2 T cell activation. *Semin Cell Dev Biol* 2018; **84**:65-74.
1139

Figure legends

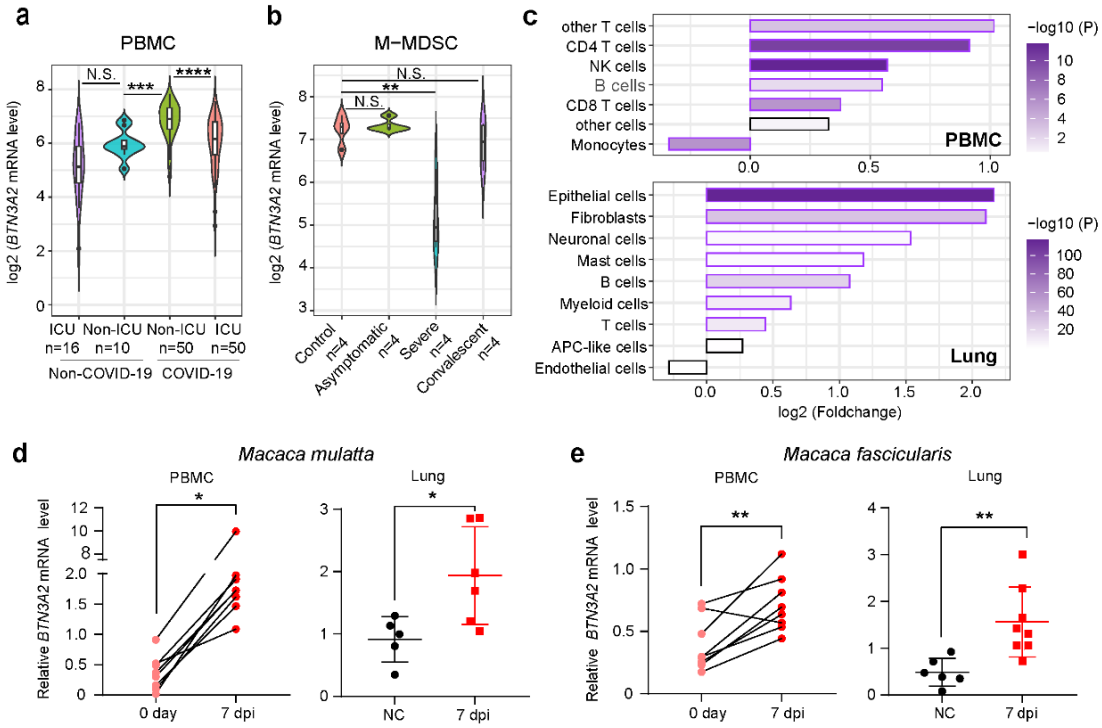

Fig. 1 BTN3A2 was up-regulated in COVID-19 patients and NHPs infected with SARS-CoV-2.

a: Violin plot of *BTN3A2* mRNA levels in peripheral blood mononuclear cells (PBMCs) from COVID-19 patients with (ICU COVID-19) or without ICU experience (Non-ICU COVID-19) compared to healthy individuals (Non-ICU Non-COVID-19) and individuals in ICU but not for COVID-19 (ICU Non-COVID-19). Original dataset (GSE157103) was reported in Overmyer et al. [51].

b: Violin plot of *BTN3A2* mRNA levels in monocytic-myeloid-derived suppressor cells (M-MDSCs) based on the GSE178824 dataset [52]. *BTN3A2* mRNA level was normalized by trimmed mean of M-values.

a-b: *BTN3A2* mRNA levels were normalized by transcripts per million (TPM). Gene expression level was determined as log2 fold-change.

c: Histogram showing up-regulation of *BTN3A2* mRNA levels in PBMCs (*upper*) and lung tissues (*lower*) of COVID-19 patients based on datasets reported in Tian et al. [57] and Melms et al. [58]. Statistical significance was assessed by two-sided Wilcox rank sum test. Purple borders indicate $P<0.05$ and black borders indicate $P>0.05$. Statistical significance was assessed by two-sided *t*-test.

d-e: *BTN3A2* mRNA levels were up-regulated in PBMCs (*left*) and lung tissues (*right*) of rhesus (**d**) and cynomolgus monkeys (**e**) challenged with or without SARS-CoV-2. For PBMCs, samples were collected before SARS-CoV-2 infection (0 day) and at 7 days post infection (dpi). For lung tissues, samples were collected from animals without SARS-CoV-2 infection (NC) and animals infected with SARS-CoV-2 at 7

1165 dpi. *BTN3A2* mRNA level was measured by qRT-PCR and normalized to *GAPDH*.
1166 Differences between two groups were determined by two-tailed Student's paired *t* test
1167 (PBMCs) and unpaired *t* test (Lung), respectively. *, $P < 0.05$; **, $P < 0.01$.
1168

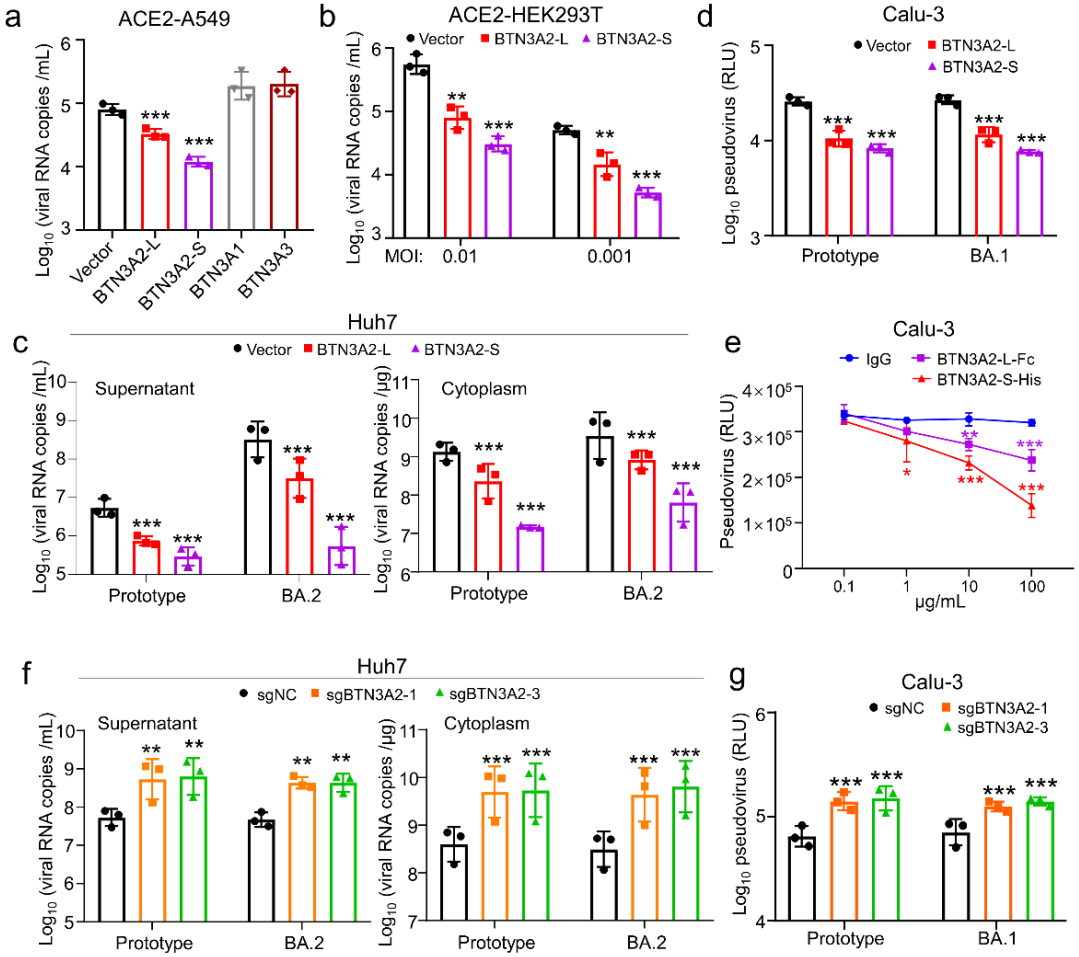

Fig. 2 BTN3A2 was identified as a potent restriction factor for SARS-CoV-2 infection.

a: Overexpression of BTN3A family members inhibited SARS-CoV-2 replication in A549 cells overexpressing human ACE2 (ACE2-A549). ACE2-A549 cells (1×10^5) were transfected with indicated expression vector (BTN3A2-L, BTN3A2-S, BTN3A1, or BTN3A3) or empty vector (Vector) (each 1 μg) for 24 h, then infected with SARS-CoV-2 (MOI=0.01) for 24 h. Cells were harvested to determine SARS-CoV-2 copies by qRT-PCR.

b: Overexpression of BTN3A2 inhibited SARS-CoV-2 replication in HEK293T cells overexpressing human ACE2 (ACE2-HEK293T). ACE2-HEK293T cells (5×10^4) were transfected with indicated expression vector (BTN3A2-L or BTN3A2-S) or empty vector (each 1 μg) for 24 h, then infected with SARS-CoV-2 (MOI=0.01 or 0.001) for 24 h and harvested for quantification of SARS-CoV-2 copies.

c: Stable expression of BTN3A2 in Huh7 cells inhibited SARS-CoV-2 replication. Huh7 cells overexpressing BTN3A2-L or BTN3A2-S, and control cells (Vector Huh7) (1×10^5 cells) were treated with DOX (1 μg/mL) for 24 h, then challenged with the SARS-CoV-2 prototype or BA.2 (MOI=1) for 24 h. The culture medium (supernatant, *left*) and cell lysates (cytoplasm, *right*) were collected to quantify SARS-CoV-2 copies.

d: Stable expression of BTN3A2 in Calu-3 cells inhibited replication of VSV pseudotyped SARS-CoV-2 (prototype and BA.1). The procedure was similar to that in (**c**). After 24h infection, cells were collected, and viral infectivity was quantified based on *Renilla* luciferase activity (RLU) using a *Renilla* Luciferase Assay Kit (Promega, Madison, WI, USA).

e: Incubation with BTN3A2 isoforms (BTN3A2-L-Fc and BTN3A2-S-His) inhibited replication of VSV pseudotyped SARS-CoV-2 (BA.1) in Calu-3 cells. IgG treatment was used as a negative control. Cells were incubated with BTN3A2 isoform or IgG for 1 h, then infected with VSV pseudotyped SARS-CoV-2 (BA.1) for 24 h and harvested to determine viral infectivity.

f: Knockout of BTN3A2 increased SARS-CoV-2 replication in Huh7 cells. Huh7 cells with BTN3A2 knockout (sgBTN3A2-1 and sgBTN3A2-3 Huh7) and control cells (sgNC Huh7) were infected with SARS-CoV-2 prototype or BA.2 (MOI=1) for 24 h, then harvested to quantify SARS-CoV-2 copies.

g: Knockout of BTN3A2 increased VSV pseudotyped SARS-CoV-2 (prototype and BA.1) replication in Calu-3 cells. The procedure for determining viral infectivity was the same as that in (**d**).

Data shown in (**b-d**) were average quantitative data from three independent experiments and were presented as mean±standard deviation (SD). Significance was determined by comparing to Vector in each group (a, b, c, and d), IgG control at each dilution (e), or sgNC in each group (f and g). *, $P < 0.05$; **, $P < 0.01$; ***, $P < 0.001$; one-way analysis of variance (ANOVA) with Dunnett's multiple comparisons.

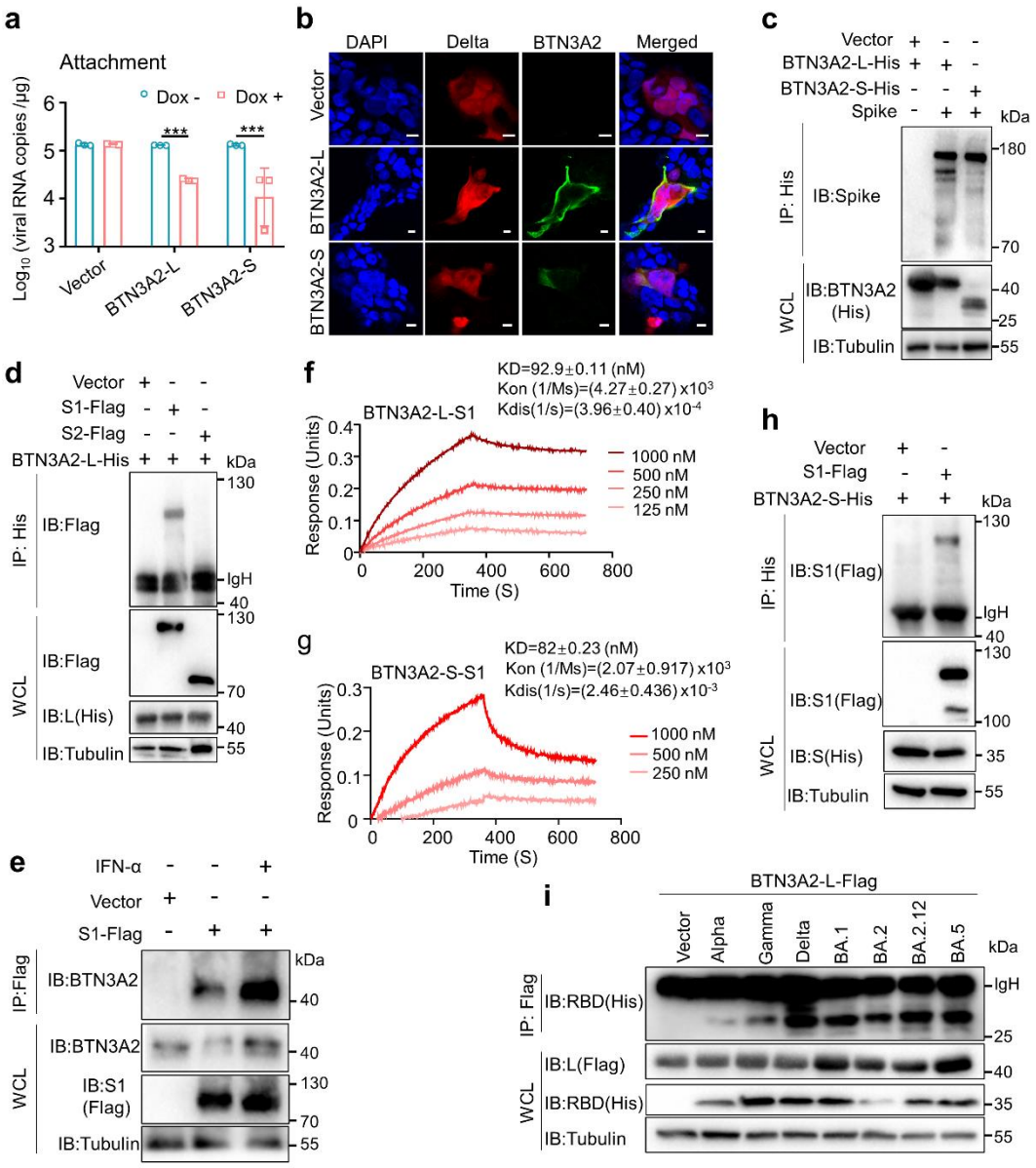

Fig. 3 BTN3A2 inhibited SARS-CoV-2 entry and interacted with Spike protein via its RBD.

a: Stable expression of BTN3A2 suppressed SARS-CoV-2 attachment to the cell. Huh7 cells overexpressing BTN3A2-L (BTN3A2-L Huh7) or BTN3A2-S (BTN3A2-S Huh7) and the control (Vector Huh7) cells were treated with DOX (1 μg/mL) for 24 h, then incubated with SARS-CoV-2 (MOI=1) on ice at 4 °C for 1 h. Cells were washed by PBS three times and harvested to measure viral RNA copies based on SARS-CoV-2 *N* gene level.

b: Representative immunofluorescence images of cell-cell fusion assay showing no apparent effect of BTN3A2 overexpression (BTN3A2-L and BTN3A2-S) on syncytia formation mediated by Spike of Delta. The HEK293T cells were transfected with Spike of Delta expression vector, and the Huh7 cells were transfected with px-300 for 16 h. The transfected Huh7 and HEK293T cells were co-cultured for 20 h and harvested for immunofluorescence assays. Scale bar, 10 μm.

c: BTN3A2 interacted with the SARS-CoV-2 Spike protein. HEK293T cells (1×10^7) were co-transfected with expression vector of BTN3A2 isoform (BTN3A2-L-His or BTN3A2-S-His, each 5 μg) and Spike protein (5 μg) for 48 h. Whole-cell lysates were immunoprecipitated (IP) using anti-His antibody. Immunoblotting (IB) for His (BTN3A2-L-His or BTN3A2-S-His), Spike, and Tubulin was performed using anti-His, anti-Spike, and anti-Tubulin antibodies, respectively.
d: BTN3A2-L interacted with the S1 subunit but not the S2 subunit of Spike protein. Spike S1 and S2 subunits were Flag-tagged.
e: Endogenous BTN3A2 interacted with the Spike S1 protein. Huh7 cells (1×10^8) were transfected with expression vector for Spike S1 protein (S1-Flag, 20 μg) or empty vector (Vector) for 36 h, then cells were treated with or without IFN-α (450 U) for 12 h. Whole-cell lysates were immunoprecipitated (IP) using anti-Flag antibody. Immunoblotting (IB) for BTN3A2, Flag (S1-Flag), and Tubulin was performed using anti- BTN3A2, anti-Flag, and anti-Tubulin antibodies, respectively.
f-g: Biolayer interferometry analyses of Spike S1 protein binding to immobilized BTN3A2-L-His (**f**) and BTN3A2-S-His (**g**). Different concentrations (1 000, 500, 250, and 125 nM, corresponding to kinetic curves from top to bottom) of Spike S1 protein were used for binding to BTN3A2-L-His and BTN3A2-S-His (lacked 125 nM), respectively.
h: BTN3A2-S interacted with the Flag-tagged S1 subunit of the Spike protein.
i: BTN3A2 interacted with Spike RBDs of different SARS-CoV-2 variants.
Procedures for IP and IB in (**d**), (**h**) and (**i**) are the same as those in (**c**).
Data are representative of three independent experiments with similar results (**b**-**i**). (**a**) Values were presented as mean±SD, and differences between groups were determined by comparing to the Dox- group; ANOVA with Dunnett's multiple comparisons, ***, $P < 0.001$.

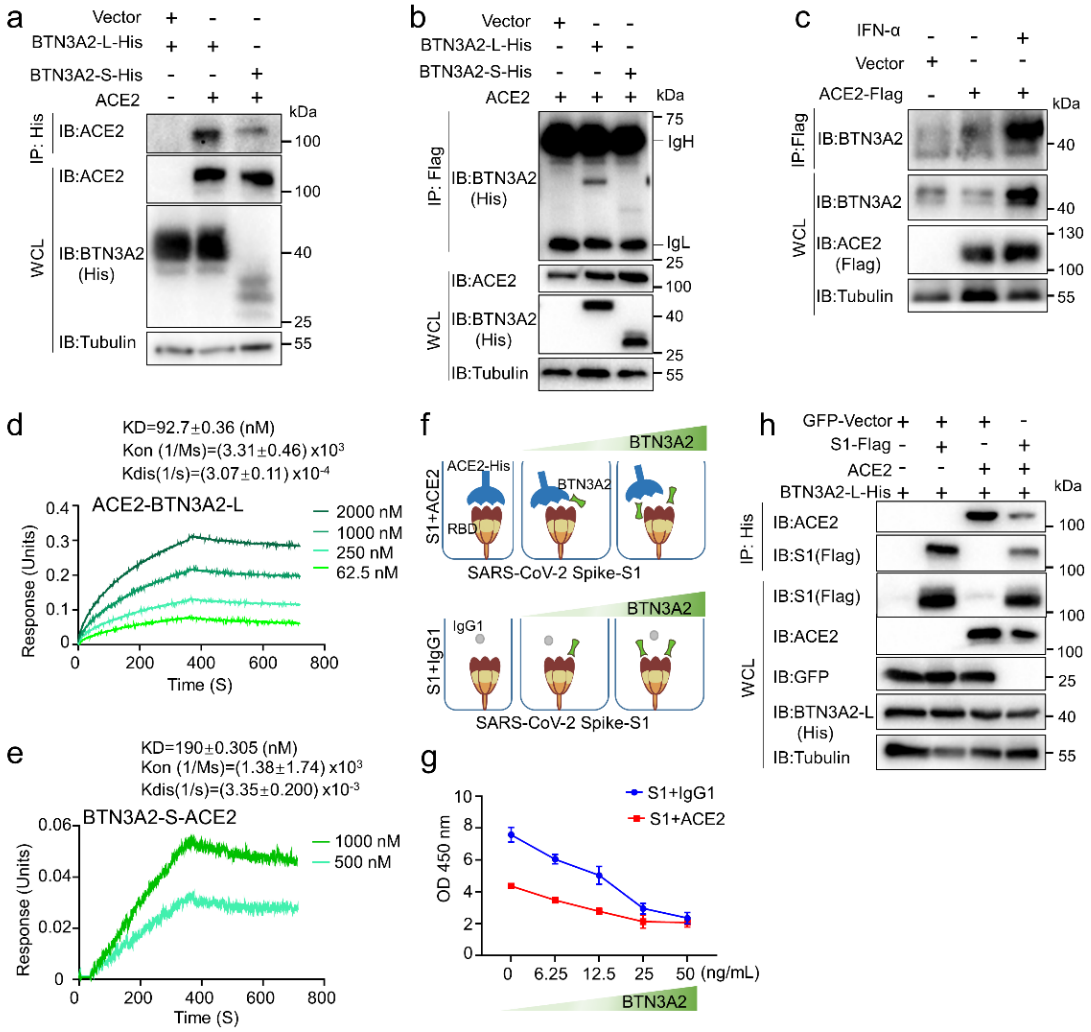

Fig. 4 BTN3A2 competed with ACE2 to bind to the Spike protein.

a: BTN3A2 isoform (BTN3A2-L-His or BTN3A2-S-His) interacted with ACE2.

b: ACE2 interacted with BTN3A2-L.

c: Endogenous BTN3A2 interacted with the ACE2. Procedures were similar to Fig. 3e.

d: Biolayer interferometry analysis of BTN3A2-L binding to immobilized ACE2-Fc. Different concentrations of BTN3A2-L (2 000, 1 000, 250, and 62.5 nM; corresponding to kinetic curves from top to bottom) were used.

e: Biolayer interferometry analysis of BTN3A2-S binding to immobilized ACE2-Fc. Different concentrations of BTN3A2-S (1 000 and 500 nM; corresponding to kinetic curves from top to bottom) were used.

f-g: Competition ELISA analysis of competitive binding of BTN3A2-L with Spike RBD (Spike-RBD). **f**: Schematic of competition assays. **g**: Competition between ACE2 (ACE2-His-tagged) and BTN3A2-L (BTN3A2) for immobilized Spike S1 subunit (S1-Fc). ACE2 and S1-Fc protein or human IgG1-Fc and S1-Fc protein were incubated for 12 h, followed by the addition of dilution series of BTN3A2-L-His. Amount of S1 protein remaining in the presence of the competitor was determined by antihuman HRP through a colorimetric readout.

h: BTN3A2-L competed with ACE2 to bind to the Spike S1. Procedures for IP and IB in (**a-b**) and (**h**) were similar to those in Fig. 3c.

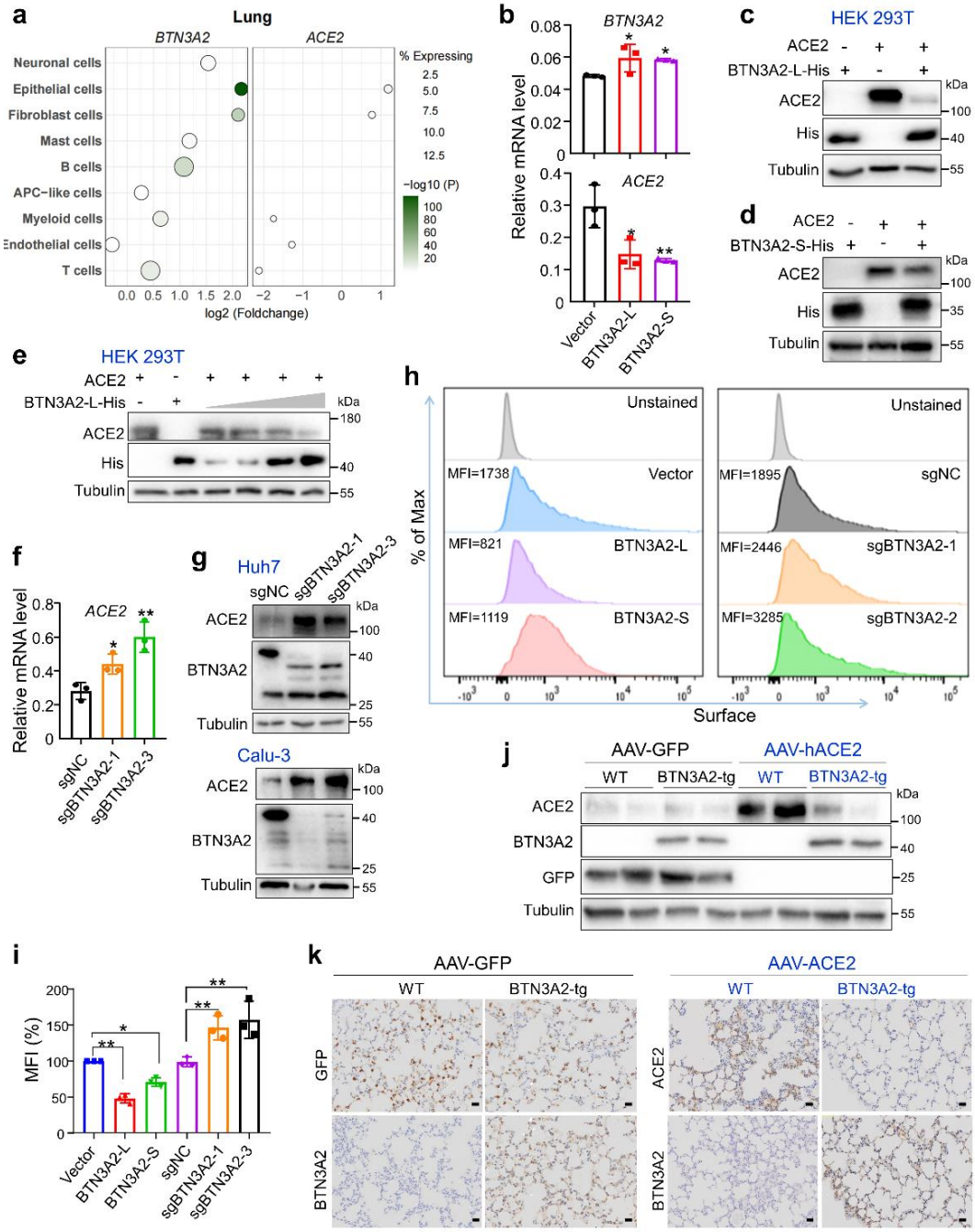

Fig. 5 BTN3A2 inhibited ACE2 expression.

a: Differential expression of *BTN3A2* and *ACE2* in scRNA-seq dataset of lung tissues from COVID-19 patients and uninfected individuals. Original dataset was reported in Melms et al. [58]. Significance was assessed by two-sided Wilcox rank sum test.

b: Stable expression of BTN3A2 decreased *ACE2* mRNA level in Huh7 cells. RNA was extracted from Huh7 cells overexpressing BTN3A2-L and BTN3A2-S, or control (Vector Huh7) cells (each group 1×10^5 cells). *BTN3A2* and *ACE2* mRNA levels were measured by qRT-PCR, with normalization to *GAPDH*.

c-d: Overexpression of BTN3A2-L (**c**) and BTN3A2-S (**d**) suppressed ACE2 protein expression in HEK293T cells. Cells (5×10^5) were transfected with indicated

expression vector or empty vector (each 1.25 μg) for 48 h, then harvested for western blotting.

e: Dose-dependent inhibitory effect of BTN3A2-L on ACE2 protein expression. HEK293T cells (5×10^5) were transfected with indicated expression vector or empty vector (each 0.5 μg), together with increased BTN3A2-L-His (0.25, 0.50, 0.75, and 1.50 μg, with empty vector to reach a total amount of 2.5 μg of plasmid) for 48 h, then harvested for western blotting.

f: Knockout of BTN3A2 increased *ACE2* mRNA level in Huh7 cells. The procedure was similar to that in (b).

g: Knockout of BTN3A2 promoted ACE2 protein expression in Huh7 (*upper*) and Calu-3 (*lower*) cells.

h-i: Flow cytometry was conducted to show surface ACE2 in Calu-3 cells with BTN3A2 overexpression (BTN3A2-L and BTN3A2-S) or knockout (sgBTN3A2-1 and sgBTN3A2-2), together with the control cells (vector and sgNC) and unstained cells. Cell surface expression of ACE2 was measured (**h**), and quantification of mean fluorescence intensity (MFI (%), n=3) was based on three independent experiments (**i**).

j: ACE2 in BTN3A2-tg and WT mice infected with indicated AAV-GFP and AAV-hACE2. Immunoblotting for ACE2, BTN3A2, GFP, and Tubulin was performed using anti-ACE2, anti-BTN3A2, anti-GFP, and anti-Tubulin antibodies, respectively.

k: Representative images of immunohistochemical staining of ACE2 and BTN3A2 in lung tissues in (**j**). Scale bar, 100 μm.

Data were representative of three independent experiments with similar results (**b-k**). Values were presented as mean±SD (**b**, **f**, and **i**). Significance was determined compared to Vector (**b** and **i**) or sgNC (**f** and **i**). ns, not significant; *, P <0.05; **, P<0.01; ANOVA with Dunnett's multiple comparisons.

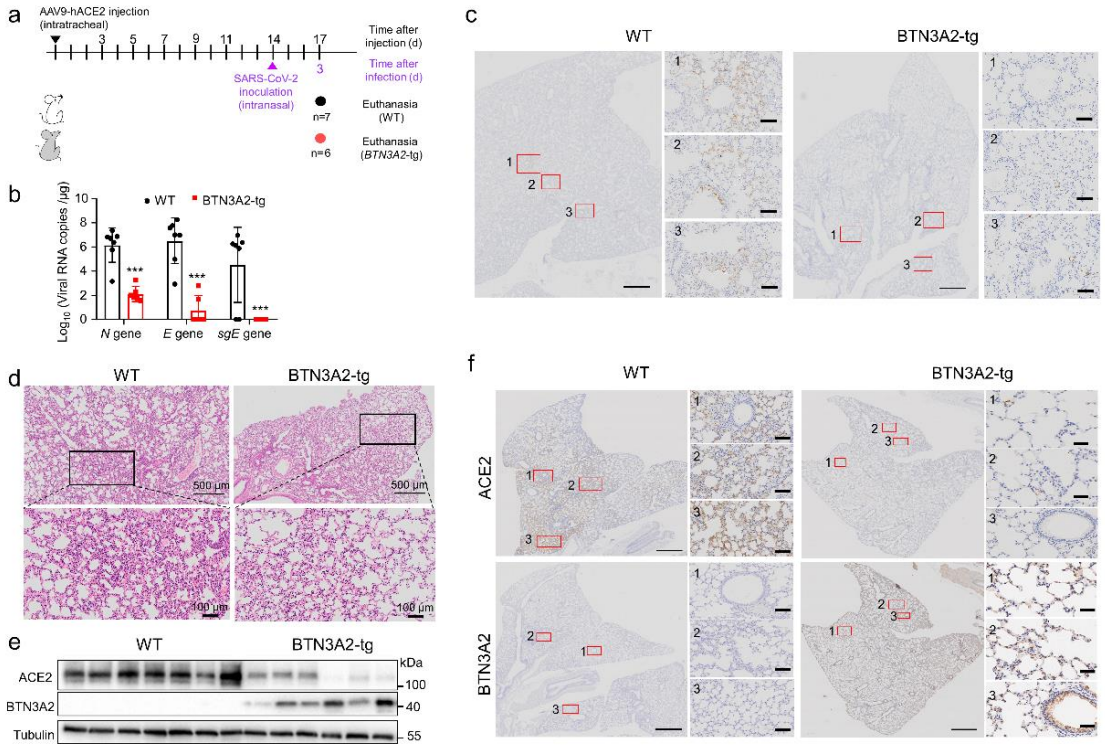

Fig. 6 BTN3A2 suppressed ACE-mediated SARS-CoV-2 entry.

a: Schematic of animal experiments with SARS-CoV-2 inoculation. BTN3A2-tg (*n*=6) and WT mice (C57BL/6J, *n*=7) were intranasally infected with AAV9-hACE2 (2×10^{12} viral genome copies) for 14 days, with all animals then infected with BA.2 (5×10^{4} $TCID_{50}$). All mice were euthanized at 3 dpi for tissue collection.

b: Viral RNA copies in lung tissues of SARS-CoV-2-infected mice at 3 dpi. Each dot indicates log copies of viral genomic N gene, E gene, and subgenomic E (sgE) of a mixed sample of five lung lobes from an individual mouse. Viral copies are presented as mean±SD. ***, $P<0.001$; ANOVA with Dunnett's multiple comparisons.

c: Representative image of immunohistochemical staining of SARS-CoV-2 N protein in lung tissues of WT and BTN3A2-tg mice at 3 dpi. Scale bars: 500 μm for entire lung lobe section (*left*) and 100 μm for enlarged view of boxed areas labeled by numbers in entire section (*right*).

d: Representative of image of H&E staining of lung sections in SARS-CoV-2-infected WT and BTN3A2-tg mice.

e: AAV-mediated hACE2 expression in lungs tissues of WT (C57BL/6J, *n*=7) and BTN3A2-tg mice (*n*=6) at 3 dpi.

f: Representative image of immunohistochemical staining for ACE2 and BTN3A2 in lung tissues of WT and BTN3A2-tg mice at 3 dpi. Scale bars were same as those in (**c**).